UNITED NATIONS EDUCATIONAL, SCIENTIFIC AND CULTURAL ORGANIZATION
INTERNATIONAL ATOMIC ENERGY AGENCY
INTERNATIONAL CENTRE FOR THEORETICAL PHYSICS
I.C.T.P., P.O. BOX 586, 34100 TRIESTE, ITALY, CABLE: CENTRATOM TRIESTE

SMR.959 - 13

MINIWORKSHOP ON STRONG ELECTRON CORRELATIONS
"Disorder and Interaction in Quantum Systems and Their Classical Analogs"

(1 - 19 July 1996)

"The Inorganic spin-Peierls compound $CuGeO_3$"

Jean-Paul Boucher
Universite' Joseph Fourier
Laboratoire de Spectrometrie Physique
38042 St. Martin d'Heres
France

These are preliminary lecture notes, intended only for distribution to participants.

Journal de Physique

The Inorganic spin-Peierls Compound $CuGeO_3$

J.P. Boucher
Laboratoire de Spectrométrie Physique
Unité Mixte de Recherche N° C5588 du
Centre National de la Recherche Scientifique
Université Joseph Fourier Grenoble I, BP 87
38402 Saint Martin d'Hères cédex, France

and

L.P. Regnault
Département de Recherche Fondamentale sur la Matière Condensée
Service de Physique Statistique, Magnétisme et Supraconductivité
Laboratoire de Magnétisme et Diffraction Neutronique
Centre d'Etudes Nucléaires
38054 Grenoble cédex, France

Abstract:

A review of recent experimental results obtained on the inorganic spin-Peierls compound $CuGeO_3$ is proposed. As the spin-Peierls phenomenon results from the interplay between lattice and magnetic (quantum) fluctuations, the presentation focuses on the different dynamical aspects of the problem. With $CuGeO_3$, many points have been clarified and new results acquired. However, it remains open questions which, due to the high quality of the available crystals, can be expected to be solved in the future.

I - Introduction

Since the pioneering work of Hase et al. in 1993 [1], a lot of works, both theoretical and experimental, has been devoted to the compound $CuGeO_3$. It is now well established that this inorganic material provides a very good example of a "spin-Peierls system". Such a system can be defined as follows: it is a spin system which undergoes lattice distortions under the effect of magnetic quantum fluctuations. This remarkable dynamical magneto-elastic phenomenon gives rise to a rather universal phase diagram as a function of field H and temperature T. Such a behavior was predicted to occur in one-dimensional (1D) Heisenberg - or XY - antiferromagnetic (AF) s = ½ spin chains [2], where, as $T \rightarrow 0$, large quantum fluctuations are known to develop in a broad continuum of excitations [3]. The first observations of spin-Peierls (SP) transitions were obtained on organic materials [4], which, in the 70's, were found to provide good examples of quasi-1D conducting and/or isolating spins systems [5]. The recent discovery of $CuGeO_3$ as a spin-Peierls system has renewed the interest in this fascinating phenomenon. Large single crystals of high quality are now available, allowing experimentalists to develop measurements which could not be done before. In the last years, many questions have been solved, new have occurred and some remain open. This explains that the research on $CuGeO_3$ is still very active. In the following, a review of recent experimental results obtained on this compound is presented.

The basic properties of the material are described in paragraph II. The (H,T) phase diagram is shown to correspond quite well to the theoretical predictions for a spin-Peierls system [6]: the characteristic three different phases are well identified (fig.1). At high temperature, there is the "uniform" U phase, where the system is usually considered to be made of simple magnetic chains (they are defined with one lattice parameter c, and one exchange coupling J_c between neighboring spins). As the temperature is decreased, a first structural transition is achieved at T_{sp} (~ 14 K in $CuGeO_3$). In moderate field, this transition corresponds to a dimerisation of the lattice. In that "dimerised" D phase, two lattice parameters and two exchange couplings J_{c1} and J_{c2} are then needed to define the magnetic chains. Increasing the magnetic field from the D phase yields a new transition occurring at a specific value H_c of the field (H_c ~ 12.5 T in $CuGeO_3$). This field-induced transition corresponds to a new deformation of the lattice. Above H_c, the lattice becomes incommensurate (with respect to the uniform and the dimerised chains). In this "incommensurate" I phase, the lattice deformation should follow the applied magnetic field until a uniform (but ferromagnetic) structure is re-obtained [6-8].

The magneto-elastic coupling which governs the different lattice distortions is generally considered under the simple form of a linear coupling between spins and phonon operators [6-8]. Such a model predicts the different structural transitions to be driven by a well defined "soft mode" of the phonon spectrum, the softening being directly induced by the magnetic quantum fluctuations. Though it is a crucial point in the problem, such a soft mode has never been observed in the past [4]. The experimental studies concerning the lattice and the phonon spectrum of $CuGeO_3$ are presented in paragraph III. The crystallographic structure of this material is shown to depend appreciably on both temperature and field. The different lattice distortions - dimerisation and incommensurability - have been clearly identified, and the associated critical, and pre-critical, behaviors are compared with the predictions of current models.

The dynamical properties of isotropic antiferromagnetic chains have always been the subject of many propositions and discussions. For spins s = ½, the prediction that, at T = 0, there ex-

ists a continuum of excitations starting from the ground state was given in 1931 (the "Bethe ansatz") [9]. For integer spins (i.e., s = 1 for instance), a completely different prediction (the "Haldane conjecture") was presented in 1983 [10]: an energy gap should exist between the ground state and the elementary excitations. In the former case, low-energy fluctuations are expected to develop as $T \rightarrow 0$, while they are suppressed in the latter case. The spin-Peierls phenomenon, which is a direct consequence of these low-energy fluctuations as they create instabilities in the whole system can only be observed in the quantum spin case. The distortion which occurs at the SP transition yields an immediate stabilization of the system, since in the case of dimerised magnetic chains, as in the Haldane conjecture, an energy gap Δ is present in the excitation spectrum [11]. The role of the magnetic excitations and fluctuations which are so essential in the spin-Peierls phenomenology will be considered in Paragraph IV. They will be analyzed in the different phases, with a particular interest on their low-energy contribution.

The experimental investigation on $CuGeO_3$ can be predicted to remain very active in the near future. Different points, which question the usual basic spin-Peierls phenomenology, are still unsolved. These points are briefly reviewed in the conclusion where a sketch of recent studies on doped samples is also given.

II - $CuGeO_3$

Germanate $CuGeO_3$ crystallizes within an orthorhombic structure of space group Pbmm. The lattice parameters at room temperature are: a = 4.81 Å, b = 8.43 Å and c = 2.95 Å. The crystallographic structure of this compound is reproduced in fig.2 [12]. It can be described as a staking of CuO_2 chains and GeO_4 chains sharing one oxygen atom. The chains are aligned along the **c** axis and the unit cell contains two unit formula. The Cu-O-Cu bonding angle (responsible for the super exchange intrachain couplings) is very near 90°, a value which should imply a strong sensitivity to distortions of the CuO_2 groups. Neutron diffraction measurements as a function of temperature down to 20 K [13] recently revealed a quite sizable and continuous structural deformation, which can be viewed as a twisting of the O(2)-O(2) octahedron edges accompanied by a translation of the tetrahedron.

The specificity of $CuGeO_3$ has been early recognized from the quite intriguing behavior observed at low temperature on the susceptibility $\chi(T)$. Figure 3 shows the first results obtained for $\chi(T)$, by Hase et al. [1]. The most remarkable feature concerns the rapid drop which is observed below ~ 14 K for any crystallographic directions **a**, **b** and **c**. Such a low-T behavior is quite reminiscent of that observed on the prototype spin-Peierls systems, like e.g. TTF-CuBDT [14] or $MEM(TCNQ)_2$ [15], and it was immediately proposed that $CuGeO_3$ is the first example of an inorganic spin-Peierls compound (with $T_{sp} \sim 14$ K) [1]. Above T_{sp}, $\chi(T)$ is essentially characterized by a maximum at $T_M \sim 60$ K (the small anisotropy is attributed to the gyromagnetic factor g of the Cu ions). Such a maximum in $\chi(T)$ is actually expected for a low-dimensional Heisenberg AF spin system. The comparison with the quantum ($s = \frac{1}{2}$) spin chain model ($T_M = 0.64J_c$) [16], yields for the nearest-neighbor (nn) intrachain exchange interaction in the U phase the following evaluation: $J_c \sim 94$ K. However, the agreement between the observed $\chi(T)$ and the Bonner-Fisher prediction [16] is rather poor. The deviation from this law occurs at relatively high temperature, typically below 200 K. Such an "anomaly" is not unique and has already been observed in other spin-Peierls systems like e.g. $(BCP\text{-}TTF)_2X$ (where $X = PF_6$ or AF_6) [17]. It may find its origin either in the existence of relatively impor-

tant magneto-elastic effects, starting well above T_{sp}, or in the existence of a non-negligible next-nearest neighbor (nnn) intrachain exchange coupling. As a support of the former assumption, it might be interesting to compare $\chi(T)$ with the T dependence observed on the lattice parameters (cf. Section III). Within the latter model, it has recently been shown that the observed $\chi(T)$ could be well explained if the ratio between nn and nnn couplings is of the order of $J'_c/J_c \sim 0.2$ with $J_c \sim 150$ K [18]. Magnetization measurements M(T) have been performed for different field values [19]. A few examples of such data are shown in fig.4 (for H applied in the **a** direction). As for $\chi(T)$, the drop in M(T) observed between 14 and 10 K characterizes the spin-Peierls transition: as expected (see fig.10 in Section III), T_{sp} is seen to decrease slightly with H increasing. In the narrow field range 12.5-13.5 T a noticeable re-entrant effect is also observed at low temperature. That increase of M(T) observed at the lowest T corresponds to the crossing of the D-U transition line. It is observed because, in $CuGeO_3$, the critical field H_c decreases slightly with T (see fig.1). Defining T_{sp} as the temperature where $\chi \sim \partial M/\partial T$ is maximum, the phase diagram given in fig.1 is finally obtained [19, 20]. As shown in fig.5, specific heat measurements $C_p(T)$ have also been performed as a function of an applied magnetic field (up to 21 T) [21]. For any value of H, the spin-Peierls transition is well characterized and clearly seen to be of second order. In contrast, according to the hysteresis observed below ~ 6 K on M(H) [22], the D-I transition is considered to be of first order. As shown in fig.6, for T ~ 1.5 K, the hysteresis is of the order of $\delta H_c \sim 0.1$ T.

The three phases characterizing a spin-Peierls system are clearly observed in $CuGeO_3$. As expected the U-D and U-I transitions are of second order, which is represented by the solid line in fig.1, while the D-U transition is of first order (the dashed line in the same figure). The Lifschift (L) point is determined for $H_L \sim 13$ T and $T_L \sim 11.5$ K. To our knowledge, the re-entrant behavior associated with the D-U transition, theoretically predicted [6-8], is observed for the first time.

III - Lattice and Phonons

Following the usual spin-Peierls phenomenology [6-8], the magnetic fluctuations present in the U phase are expected, via some spin-phonon couplings, to induce drastic changes in the lattice properties. Indeed, a major feature concerns the appearance of a lattice dimerization, at least when the applied magnetic field is not too large. In stronger fields however, an incommensurate distortion is expected to occur, below T_{sp}. Such lattice distortions should be characterized by the occurrence of super-lattice peaks in addition to the "normal" Bragg peaks in reciprocal space. These additional peaks are described by a 3-dimensional (3D) propagation vector hereafter labeled $\mathbf{k}_{sp}$. Such lattice distortions should result also in appreciable changes in the spin dynamics, which are considered in next Section.

A - Lattice distortion in zero field:

In $CuGeO_3$, the rapid drop observed on the susceptibility $\chi(T)$ below 14 K [1] is clearly associated with appreciable temperature dependencies of structural components, which reveal that sizable magneto-elastic couplings exist in this compound. Figure 7 shows the temperature dependence of the coefficients α_a, α_b and α_c of the linear thermal expansion for the three crystallographic axes and, of $(\alpha_a + \alpha_b + \alpha_c)$ for the volume expansion [23]. Quite unambiguously, these measurements give evidence for a structural phase transition at $T_{sp} \sim 14.3$ K. They also show that, well above T_{sp}, the lattice of $CuGeO_3$ is already very sensitive to tem-

perature (it is interesting to compare fig.3a and fig.7, for instance). All these results are corroborated by X-ray [24] and neutron diffraction [25, 26] measurements. The temperature dependence of the lattice parameters a, b and c are reported in fig.8. The largest variation is definitely observed along the b-direction, where a well defined drop of the lattice parameter is clearly seen below T_{sp}. X-ray [27], neutron [26-28] and electron [29] diffraction measurements have provided a precise determination of the structural distortion occurring at T_{sp}. The first evidences of the existence of superlattice peaks below T_{sp} were obtained from X-ray [27] and electron [29] diffraction measurements. These satellites have been indexed with a commensurate propagation vector $\mathbf{k} = [1/2,1,1/2]$, corresponding to out-of-phase displacements from the original atomic positions. Neutron diffraction measurements on a single crystal have confirmed the presence of such nuclear satellites not only for odd [26,27] but also for even k_b components [26], a fact which indicates that the actual propagation vector in $CuGeO_3$ is $\mathbf{k}_{sp} = [1/2,0,1/2]$. The location of the corresponding point in reciprocal space is given in fig.9a. Figure 10a shows a typical longitudinal scan through the satellite observed at [1/2,3,1/2], which gives evidence for a resolution-limited peak. The purely nuclear nature of these superlattice peaks has been established from both their scattering wavevector **k** and temperature T dependencies. The T dependence of the [1/2,3,1/2] satellite is depicted in fig.10b. As can be seen, the Bragg-peak intensity vanishes at T_{sp}, exactly where the drop in the susceptibility $\chi(T)$ occurs. The observed behavior is consistent with a critical exponent $\beta \sim 0.27\text{-}0.30$, an evaluation far from the mean-field prediction $\beta \sim 0.5$ [28]. This small value of β however agrees with the fact that, above T_{sp}, appreciable anisotropy is present in the structural fluctuations. Although hardly visible in the neutron scattering measurements [30], these fluctuations have been clearly observed by X-ray diffraction, up to ~ 50 K [27]. Figure 11 shows the temperature dependence of the structural inverse correlation lengths ξ^{-1} measured along the three reciprocal directions **a***, **b*** and **c*** [27, 31]. Within experimental errors, ξ_c^{-1} becomes 3D near T_{sp} and behaves as $(T- T_{sp})^{1/2}$, whereas, as T increases, the pre-transitional fluctuations are seen, in the **a** and **b** directions, to become successively uncoupled.

An accurate determination of the crystallographic structure of the dimerised phase (i.e., for $T < T_{sp}$) has been obtained from neutron diffraction measurements performed on series of satellites [27, 13]. The corresponding lattice distortion is reported in fig.12. According to that model, the largest displacements are observed for the Cu-atoms which move along the **c** axis, and for the O(2)-atoms which move in the (**a**,**b**) plane, however with very small relative values [13]: $u^c_{Cu}/c \sim 0.0020$, $u^a_{O(2)}/a \sim 0.0018$ and $u^b_{O(2)}/b \sim 0.0008$. The resulting lattice distortion can be described as an alternating rotation of the GeO_4 groups around the Ge atoms [27] or around the O(1)-O(1) axis [13], which alternately induces positive or negative displacements of Cu atoms along **c**, and eventually a small displacement of Ge atoms along **b** [13]. Such small displacements explain, even quantitatively, how difficult is the detection of pre-transitional structural fluctuations from neutron diffraction, except very near T_{sp} [30]. For the same reason, and despite very careful measurements [25, 32-36], performed in particular in the vicinity of $\mathbf{k}_{sp}$, it has not been possible so far to observe any phonon softening when approaching T_{sp}. Examples of phonon dispersion curves measured in the [0 0 1] and the [1 0 1] directions [33] at room temperature are shown in fig.13. Only very weak changes are observed as T decreases, even for $T < T_{sp}$ (after corrections due to the usual Bose factor). No phonon softening has yet been detected in $CuGeO_3$. This negative result may be attributed either to the weakness of the relevant phonon intensity or to the nature of the phase transition itself (see Conclusion).

B - Lattice distortion in a field:

In the D phase, the structural properties are expected to be little affected by the application of a magnetic field, at least up to the critical value H_c, above which begins the incommensurate I phase. According to the usual descriptions, H_c is directly related to the transition temperature T_{sp} and the spin-gap Δ expected to characterize the magnetic excitation spectrum of dimerised chains [11] (cf. Section IV):

$$H_c \sim 1.48\ kT_{sp}/g\mu_B \sim 0.84\ \Delta/g\mu_B,$$

and, in low fields, T_{sp} should decrease quadratically with H [7, 8]:

$$\Delta T_{sp}/T_{sp} \sim - t\ \{g\mu_B H/[2\ kT_{sp}(0)]\}^2$$

Different techniques including X-ray [24], magnetization [37], ultrasonic studies [38, 39] and neutron scattering [28] have shown that such a behavior is well observed in $CuGeO_3$. Figure 10b gives the evolution with temperature of the maximum intensity of the satellite [1/2,3,1/2], for two values of the magnetic field, H = 0 and H = 9.85 T. As expected, $T_{sp}(H)$ displays a slight decrease, of about 13 % in this field range. The corresponding experimental data are summarized in fig.10c. They are well reproduced by the above quadratic relation, but with a pre-factor t ~ 0.5, slightly larger than the theoretical evaluations, t ~ 0.36 - 0.44 [7, 8]. This discrepancy can be attributed to the precursor low-D structural fluctuations (fig.11), which are neglected in the usual theoretical approaches based essentially on mean field approximations.

In a field, the most interesting feature is expected to occur above the critical field H_c, in the I phase. The lattice incommensurability characterizing that phase has been proposed to be described by a soliton-lattice model [40-43], associated with a field-dependent incommensurate wave vector $\mathbf{k}_{sp}(H)$. In the simplest case, the lattice distortion can be viewed as a staking of dimerized regions regularly spaced by a 3-dimensional array of domain walls (i.e. the "solitons") carrying each one a spin 1/2. The magnetization recovered above H_c is then directly related to the number of solitons. The cell parameter L of the soliton lattice (representing two times the soliton-soliton distance) is directly related to the departure from the commensurate wavevector $\mathbf{k}_{sp} = \mathbf{k}_{sp}(0)$, namely:

$$|\mathbf{k}_{sp}(H) - \mathbf{k}_{sp}(0)| \sim 2\pi / L \propto M(H)$$

This quantity would be an increasing function of field, whereas the soliton half-width Γ should be weakly field dependent [40-43]. Moreover, the Fourier transform of the lattice distortion is expected to contain only odd harmonics ($\pm 3\ \mathbf{k}_{sp}$, $\pm 5\ \mathbf{k}_{sp}$,...), with rapidly decreasing amplitudes [43]: the lattice modulation should be nearly sinusoidal.

X-ray diffraction measurements [44, 45] have recently confirmed the incommensurate nature of the I-phase in $CuGeO_3$. Figure 14a shows series of wavevector scans through the [5/2,1,5/2] satellite performed in the [1 0 1] direction, for fields below and above the critical field H_c. At low field, a two-peak structure is observed, which is due to the use of an incident X-ray beam containing two different wavelengths. Above H_c, each peak is seen to split into

two satellites, giving rise finally to a four-peak structure. For these satellites, the component of $\mathbf{k}_{sp}(H)$ along the chain axis is seen to become incommensurate. The intensity of both the commensurate and incommensurate reflections are given as a function of field in fig.14b. Two important features of the D-I transition emerge from the present data obtained on pure $CuGeO_3$: the step-like behavior at H_c and the relatively weak hysteresis $\delta H_c \sim 0.1$ T, the latter effect being also reported from magnetization measurements (see fig.6) [22]. Both results are signatures of the first-order character of the phase transition at H_c, which would suppose a "pinning" of the solitons. The incommensurability along the chain is observed to increase with H, which, in the soliton model, corresponds to a decreasing soliton distance. The recent observation, by X-ray diffraction [45], of a tiny third-order-harmonic satellite (with relative intensity $I_3/I_1 \sim 1/(100\text{-}150)$ strongly supports the soliton-lattice model for $CuGeO_3$. A soliton width could be evaluated. Along the chain, the relative half-width is of the order of $\Gamma/c \sim 10\text{-}15$, which implies a non-negligible overlap of the domain walls. Finally, in the limited explored field range (between H_c and 13 T), Γ is observed to be practically field independent, as expected.

IV - Magnetic Excitations and Fluctuations

A - The dimerised D phase:

The investigation of the magnetic excitations in the D phase is important for two reasons. As explained in the introduction, an energy gap Δ should be seen in the energy spectrum [11] and, in such a dimerised phase, the effect of a magnetic field should reveal a very peculiar behavior. This latter point is a general feature of the so-called "spin-liquid systems" [46], whose dimerised and Haldane spin chains belong to. In such systems, the elementary excitations are actually defined with an additional quantum number S = 1, where S represents the total spin operator. Due to this property, the application of a magnetic field should result in a Zeeman splitting of the elementary excitation spectrum, and, additionally, specific low-energy fluctuations should develop in the spin system.

In the D phase of $CuGeO_3$, well defined excitations have been observed by neutron inelastic scattering (NIS) measurements [47, 28]. For H = 0, the corresponding dispersion curves are shown in fig.15. In that figure, the value q (or q_b or q_c) = 0 refers to the point [0,1,1/2] of the 3D reciprocal space given in fig.9a. It corresponds to the AF wavevector for the spin system: $\mathbf{k}_{AF}$ = [0,1,1/2]. Dispersive effects are clearly observed in the three crystallographic directions. From these curves, a determination of the magnetic couplings both along and perpendicular to the chains can be made [47, 28]. In fig.16b, the data obtained along $\mathbf{c}^*$ are compared (the full line) with the usual expression for dimerised chains (with magnetic alternation $\alpha = J_{c2}/J_{c1}$) [11]

$$E_q = [\Delta^2 + (E_M^2 - E_G^2)\sin^2(2\pi q_c)]^{1/2}$$

where Δ [$\sim 1.05\ J_{c1}(1 - \alpha)^{2/3}$] is the expected energy gap [48] and $E_M = \pi J_{c1}(1 + \alpha)/4$ represents the maximum energy in the dispersion: $E_M \sim 15$ meV (~ 170 K) K. For J_{c1} and α, one then obtains the following evaluations: $J_{c1} \sim 122$ K and $\alpha \sim 0.92$ [28]. For small values of q_c, the agreement between that model and the data is however only approximate. The dashed line shown in the same figure would better evaluate the effective velocity ($v \sim 157$ K) of the elementary excitations. With $v = \pi J_c/2$, as for uniform chains [3], one would obtain an "apparent" exchange coupling $J_c \sim 100$ K [28]. Finally, it is worth mentioning that, if a next-neighbor

interaction (J'_{c1}) along the chain is taken into account, the slight misfit observed at low values of q_c is reduced. Within a simple Holstein-Primakoff procedure, a good agreement with the data can be obtained for $J'_{c1}/J_{c1} \sim 0.17$ [49]. The value of this ratio compares well with that ($J'_c/J_c \sim 0.2$) of the recent model proposed for analyzing the susceptibility in the U phase (see Section 2 and [18]). For the dispersion along **b***, the neutron data are shown in fig.15c. They are compared with a standard "spin-wave" model (full line), which yields, for the exchange coupling in the **b** direction, $J_b \sim 10$ K. Similar analysis performed along **a*** gives $J_a \sim 1$ K [34, 28].

Due to these interchain couplings, several gaps can therefore be observed in the whole 3D reciprocal space. However, neglecting the rather small dispersion along **a***, essentially two gaps have to be considered. The lowest energy gap, $E_{G1} = 2 \pm 0.05$ meV (= 23 ± 0.6 K), occurs, in particular, at the antiferromagnetic wavevector $\mathbf{k}_{AF} = [0,1,1/2]$, and the largest, $E_{G2} = 5.7 \pm 0.25$ meV (= 66 ± 3 K), at the center of the Brillouin zone, i.e.; at $\mathbf{k}_0 = [0,0,0]$. A sketch of the dipersion curves with these different gaps is given in fig.9b. The spin-Peierls gap Δ of the usual 1D models is identified to the lowest energy gap E_{G1}, i.e.; in $CuGeO_3$, $\Delta \equiv E_{G1} \sim 23$ K.

Raman scattering measurements have been shown to offer an interesting way of probing the magnetic fluctuations in $CuGeO_3$ [50]. That technique is basically sensitive to the density of states and, accordingly, any maximum or minimum present in the excitation spectrum should result in a "peak" in the observed Raman intensity. For the dimerised D phase, the Raman data are shown in fig.16a. With respect to NIS data, a factor two occurs in the energy scale: it results from the fact that 4-spin (and not 2-spin) correlation functions are probed in a magnetic Raman process [51]. Peak I, at $E \sim 32$ cm^{-1} (~ 46 K) is therefore seen to correspond very well to the lowest energy gap E_{G1} ($2E_{G1} = 46$ K). Peak 2 was attributed to a "Fano" mode [52] resulting from a strong coupling between a phonon and the magnetic excitation continuum, rather than to the highest gap E_{G2}, which due this effect is not easily visible. Peak 3, however, occurring at ~ 230 cm^{-1} (~ 330 K) is clearly the signature of the maximum E_M ($2E_M \sim 340$ K) of the magnetic dispersion curves as they are observed in NIS measurements.

Due to the additional quantum number S = 1 mentioned above, one expects the application of a magnetic field to result in a Zeeman splitting of the elementary excitation branches. The first evidence of such an effect was obtained by electron spin resonance (ESR) measurements [22]. "ESR transitions" are defined as transitions associated with a change $\Delta m = 1$ of the magnetic quantum number, but with no wavevector transfer, i.e., $\Delta\mathbf{q} = 0$. In dimerised chains, two kinds of such transitions can be induced, between excited states and from the groundstate. Transitions between excited states can be realized in any points of the Brillouin zone and, in particular, at the lowest gap positions. As shown previously for Haldane spin chains [53], such transitions correspond to the "standard" ESR signals observed at the Zeeman frequency (for isotropic systems as $CuGeO_3$, $\nu \sim g\mu_B H$) [54]. The temperature dependence of such ESR signals is characteristic of an activated process. Assuming a Boltzmann distribution between the Zeeman split states, the data for the integrated intensity of this "standard" ESR line are well explained by this model (the full line in fig.17a) [20]. An evaluation of the lowest energy gap of the system can then obtained: $\Delta \sim 23.5$ K, which is in remarkable agreement with the NIS determination for E_{G1}. Since, in dimerised chains, the groundstate is a S = 0 state, ESR transitions can also be induced from the ground state, at least if $m = \pm 1$ excited states are also present at the Brillouin zone center ($\mathbf{k}_0 = [0,0,0]$). This is actually the case in dimerised chains

[11]. A few examples of such ESR signals observed in $CuGeO_3$ are shown in fig.17b. The extrapolation to zero field provides a direct evaluation of the gap at $\mathbf{k}_0$. The obtained value ~ 1340 GHz (~ 64 K) agrees well with the NIS determination of the second energy gap (E_{G2} ~ 66 K). This ESR investigation confirms the representation of the elementary excitations given in fig.9b. It proves also that, in a field, a Zeeman splitting does occur at the Brillouin zone center (i.e., at $\mathbf{k}_0$ = [0,0,0]) [22]. Directly observed by NIS measurements [28, 55], a similar Zeeman splitting has been shown to develop at the antiferromagnetic point $\mathbf{k}_{AF}$ = [0,1,1/2]. Such data obtained up to about 10 T [28], are displayed in fig.17c.

The additional low-energy fluctuations associated with the S = 1 quantum number were first predicted for Haldane spin chains [56, 57]. Associated with two elementary excitations of energy E_{q1} and E_{q2}, they result from transition processes involving the energy difference E_{q1} - E_{q2}. For that reason, they form a low-energy continuum, which, in zero field, spreads around E ~ 0. In the dimerised phase of $CuGeO_3$, these fluctuations have been shown [58] to contribute dominantly to the nuclear relaxation rate ($1/T_1$) of the Cu nuclear quadrupole resonance (NQR) [59] (see fig. 18). Due to these processes, $1/T_1$ is expected to decrease exponentially as a function of the gap Δ and T according to the general law ~ exp(-Δ/T) [56, 57]. Such behavior explains rather well [58] the NQR results measured in the dimerised phase of $CuGeO_3$.

B - The D-U transition:

While gaps are definitely present in the D phase, no spin gap is expected in the U phase. The D-U transition should therefore be associated with drastic changes in the magnetic fluctuation spectrum. Its evolution observed near the antiferromagnetic point $\mathbf{k}_{AF}$ [28] is shown in fig.19a. While well defined excitations are observed in the D phase (see the data at 1.8 K, for instance), a broadening and a shift of the mode is observed when approaching T_{SP} (~ 14 K). In the U phase, only a broad continuum remains, widely spread around zero energy. The corresponding critical behavior can be characterized by two quantities, the peak position (i.e. the SP gap Δ) and the energy width (or the damping parameter Γ). They are plotted as a function of temperature in fig.19b. Concerning the spin system, the dynamical D-U critical regime in $CuGeO_3$ is seen to develop, around T_{SP}, in a rather narrow temperature range (ΔT^c_{SP} ~ ± 2 K).

C - The uniform U phase:

The descriptions proposed for the SP transition are usually derived for 1D spin systems [2, 8]. In that case, a quantum (s = ½) Heisenberg hamiltonian is predicted to display very specific dynamical properties [3]. As a function of temperature, two distinct regimes have to be considered: the short range order (SRO) regime for T < T_M (~ 60 K), and the high temperature (HT) regime for T > T_M. In $CuGeO_3$, despite the presence of interchain couplings, which is well established for the D phase (see above), all the experimental results give the U phase a dominant 1D and isotropic character. Any interchain (and/or anisotropic) effects can be considered as small perturbations with respect to that 1D model. In the following, we therefore refer to a 1D reciprocal space defined by one-component wavevector: $\mathbf{q}_c$ (with -½ ≤ q_c ≤ ½ in the first Brillouin zone).

In the SRO regime, the T = 0 fluctuation spectrum of a 1D quantum Heisenberg hamiltonian (i.e. defined with one exchange coupling J_c) is represented in the inset of fig.20a. It is characterized by a continuum of propagative excitations comprised between the two dispersive lim-

its: $E'_q = \pi J_c/2 \sin(2\pi q_c)$ and $E^2_q = \pi J_c \sin(\pi q_c)$ [3]. At finite temperatures, the fluctuation modes around the AF point (i.e., $q_{AF} = 1/2$) are predicted to be overdamped by thermal fluctuations ($\Delta E \sim T$) [60]. By contrast, no such a damping is expected around the Brillouin zone center (i.e., $q_0 = 0$) [61]. At intermediate wavevectors, for $q_c \sim 1/4$ for instance, the excitation spectrum should be peaked at an energy $E'_M \sim \pi J_c/2$.

In the SRO regime, the fluctuations associated with modes near the AF point ($\mathbf{q}_c \sim \mathbf{q}_{AF}$) have been carefully analyzed by INS measurements [62]. A typical energy scan, for T ~ 15 K, is shown in fig.21. The existence of a broad continuum is clearly established and the damping observed at low energy (E ~ 0) is in very reasonable agreement with the predicted thermal effect [60]. For the fluctuations near $q_c \sim 1/4$, we refer to recent Raman scattering measurements. In fig.16b, a peak (shown by the arrow) is seen in the Raman intensity at E ~ 230 cm^{-1} (~ 330 K). This peak is to be related to the maximum (E'_M) of the dispersive limit E'_q (see above and fig.20a). From the theoretical expression, $2E'_M \sim \pi J_c$, one obtains another evaluation of the exchange coupling in the U phase, $J_c \sim 100$ K, which agrees very well with the determination ($J_c \sim 94$ K) obtained previously from T_M (see Section II). It is worth noting that, in the D phase, peak 3 (fig.16a), which corresponds also to high energy propagative excitations, occurs at the same energy value, while the exchange coupling in the dimers was evaluated to be larger, $J_{c1} \sim 122$ K. As the temperature is increased (see fig.16b), the intensity of that Raman peak decreases rapidly, to vanish at $T_M \sim 60$ K. This is in agreement with the fact that no propagative modes are expected to exist in the HT regime. However, for $T > T_M$, important fluctuations are seen to develop at low energy (see fig.16c). The diverging-like behavior observed as $E \rightarrow 0$ is characteristic of low-dimensional diffusive processes [63]. Such a diffusion is confirmed by the observed T dependence, which compares well with the evolution expected for a 1D classical spin model [64, 50].

Concerning the effect of a magnetic field in the U phase, the main effect to be mentioned in relation with the SP transition, is the magnetic incommensurability predicted to occur in the excitation spectrum of the SRO regime [3]. For $H \neq 0$, a distinction is now to be made between fluctuations parallel ($S_{//}$) and perpendicular ($S_\perp$) to the field direction. The corresponding (T = 0) theoretical predictions are sketched in figs20b and 20c. For $S_{//}$, the incommensurability occurs near the AF point $q_{AF} = 1/2$: the zero energy fluctuations are seen to be shifted out of the AF point by $\delta q_{AF} = 2\sigma$, where σ is the uniform magnetization per spin [3]. At finite temperature however, a thermal damping, as previously described for H = 0 [60], is to be taken into account. As a result, at q_{AF}, an effective incommensurability can be achieved only in large field, when the Zeeman energy overcomes the thermal fluctuations, i.e.; for $g\mu_B H \geq kT$. It is worth noting that this condition starts to be fulfilled only above the Lifschift point ($H_L \sim 13$ T, $T_L \sim 11.5$ K). Such dynamical incommensurability expected for quantum Heisenberg spin chains has not been observed in $CuGeO_3$ (nor in any other systems actually). For $S_\perp$, the incommensurability is seen to develop near the Brillouin zone center, i.e., at $\mathbf{q}_c \sim \mathbf{q}_0 = 0$. The zero-energy mode is seen to be shifted by $\delta q_0 = 2\sigma$, and the uniform ($\mathbf{q}_0 = 0$) mode by $\delta E = g\mu_B H$ [3]. Since, for such low-q values, no thermal damping is expected to happen [61], the corresponding excitation modes should remain well defined. This is actually the case, at least for the $\mathbf{q}_0$ mode, which is directly probed by ESR measurements [54, 20]. For any values of the field, a narrow ESR line is actually observed in the SRO regime: at T ~ 20 K, the ESR width is $\Delta H \sim 3$ mT [54] in low field (H ~ 0.3 T), and becomes only $\Delta H \sim 58$ mT in large field (H ~ 17 T) [20].

In the U phase of $CuGeO_3$, all the results concerning the spin dynamics agree quite well with the predictions given for Heisenberg quantum spin chains. In particular, the low-energy fluctuations which characterize such systems are seen to be transferred from $\mathbf{q_0}$ to $\mathbf{q_{AF}}$, as T decreases below T_M.

D - The incommensurate I phase:

In the I phase, the lattice of $CuGeO_3$ becomes incommensurate as established experimentally [44,45]. As seen in Section III, the corresponding lattice distortion, which is 3D, can be described in terms of solitons [40-43]. In such models, the deformation of the magnetic chains would result in dimerised segments, separated by localized domains walls, the solitons. These solitons, which allow alternation in the dimerisation, are expected to give the local magnetization [or the local susceptibility] a very specific distribution M(r) [or $\chi(r)$] along the chains [43]. Nuclear magnetic resonance (NMR) measurements, as they probe the magnetization locally - at the different Cu sites actually - have provided a direct evidence of this spatial distribution [65]. For example, starting from the ^{63}Cu NMR lineshape recorded at 1.4 K in a field H ~ 16.3 T, shown in fig.22 (lower part), one obtains for $\chi(r)$ the distribution represented in the upper part (and fitted by the solid line) of the same figure. Such a non-uniform magnetization - compare with the dot-dashed vertical line which corresponds to the magnetization expected in the U phase for the same field value - requires a pinning of the magnetic modulation, which should be that of the solitons.

Concerning the magnetic fluctuations in the I phase, very little is known. No explicit theoretical description has really been given for the spin dynamics, and only very few experimental results are available. For $CuGeO_3$, two results can be discussed, obtained from Raman scattering [66] and ESR measurements [67]. By Raman scattering it has been established that, in that high field phase, propagative - or quasi-propagative - excitations remain present at high energy. As shown by the arrow in fig.16d, for H = 20 T and T = 4.2 K, a well-defined peak is again observed in the Raman intensity at E ~ 230 cm-1 (~ 330 K). This peak is very similar (lineshape and energy position) to the peaks observed in the U and the D phases (a comparison is directly made with the peak in the D phase), and we may infer that, in the three U, D and I phases, similar dispersions govern the high energy modes. Concerning ESR, as discussed above, the signal in the U phase is to be identified with the uniform $\mathbf{q_0} = 0$ mode of the transverse fluctuations ($S_\perp$). The measurements performed at H ~ 17 T and T ~ 20 K - i.e., in the U phase - have been extended to lower temperatures down to the I phase (see fig.23). Remarkably, the ESR signal is seen to remain almost identical when the U-I transition line is crossed (with no appreciable change at $T = T_{sp}$ ~ 10 K!) [67]. This continuity observed on the ESR lines might suggest an identical origin for the uniform $\mathbf{q_0}$ mode in the two phases. From these two - Raman and ESR - results, we can only conclude that, as long as the spin dynamics is concerned, the U and I phases display evident similarities. An important question however remains about the low-energy (E ~ 0) fluctuations. Are they present in the I phase? Are they involved in the field-dependent lattice distortion which characterizes this phase? Finally, concerning the ESR line, it is worth mentioning that, at the lowest temperatures, hysteresis are observed on both the position and the linewidth (see fig.23 and [66]). In the soliton picture given above, this hysteresis could be well related to the pinning of the solitons.

V - Conclusion

In the spin-Peierls phenomenology, the fluctuations are expected to play an essential role [6-8]. As shown in the present work, they have been widely investigated in $CuGeO_3$, and new results have been obtained. Concerning the lattice, well above the spin-Peierls transition, precursor effects are clearly seen on the crystallographic parameters and, at T_{sp}, the lattice fluctuations display an evident 3-D character. Concerning the spin system, in the U phase, the fluctuations correspond rather well to what is expected for 1D systems. In particular, near T_{sp}, the AF fluctuations agree well with that picture of a thermally overdamped continuum. All these results are in agreement with the basic requirements for a spin-Peierls transition. However, the most crucial point, the dynamical interplay between spins and phonons, has not been established. In the standard models, a "low coupling" approximation is usually assumed between spins and phonons. As a result, the crystallographic distortions are expected to be driven by a well-defined soft mode. Such a soft mode in the phonon spectrum has not been observed so far, and the question on the validity of such approaches remains open. In the past, it has already been suggested that it might be worth reconsidering the SP problem beyond this approximation [68]. Finally, the nature of the phase transition itself can be questioned. Could the structural transitions be of order-disorder type, which would suppose the phononic contribution to be rather damped above T_{sp} (i.e., difficult to observe)? Anyhow, the investigation of the lattice dynamics in $CuGeO_3$ needs to be pushed further. The high quality of the crystals let us hope that a definitive conclusion on this crucial point can be reached in the future. The D and I magnetic phases have been quite well investigated. In the D phase, the elementary excitations have been accurately determined, as well as their specific properties resulting from this additional quantum number S = 1. In this way, $CuGeO_3$ appears therefore to be also a good example of a "spin liquid" system. Concerning the spin dynamics, the I phase remains widely unknown. If the lattice incommensurability is now well established, the low-frequency part of the magnetic fluctuation spectrum remains to be determined. Is there a gap or not? In the latter case, how does the spectrum compare with that of the U phase when a strong magnetic field is present, i.e., when a magnetic dynamical incommensurability exists? Finally, is there any relation between these two incommensurabilities, the magnetic incommensurability in the U phase and the lattice incommensurability in the I phase? As shown in the present work, the experimental (and theoretical) potentialities of $CuGeO_3$ are rather broad. In this respect, we can mention also the effect of dopings [69, 70]. As an example, the phase diagram as a function of the concentration x of Si atoms with respect to Ge atoms is given in fig.24. T_{sp} is observed to be drastically reduced as x increases, destroying finally the spin-Peierls transition [69]. The questions raised by such doping effects in $CuGeO_3$ opens another wide field of research for this compound.

References:

[1] - M.Hase, I. Terasaki and K. Uchinokura, Phys. Rev. Lett. **70**, 3651 (1993).
[2] - P. Pincus, Solid State Communications **9**, 1971 (1971); E. Pytte, Phys. Rev. **B10**, 2039 (1974).
[3] - G. Muller, H. Thomas, H. Beck and J.C. Bonner, Phys. Rev. **B24**, 1429 (1981).
[4] - For reviews see: D. Bloch, J. Voiron and L.J. de Jongh, in *Proceedings of the International Symposium on High Field Magnetism*, edited by M. Date (North-Holland, Amsterdam, 1983), p. 19; J.W. Bray, L.V. Interrante, I.S. Jacobs and J.C. Bonner, in *Extended Linear Chain Compounds*, edited by J.S. Miller (Plenum Press, New York, 1983), Vol.**3**.
[5] - I.F. Shchegolev, Physica Status Solidi A **12**, 9 (1972).
[6] - L.N. Bulaevskii, Sov. Phys. JETP **16**, 685 (1963); M.C. Cross and D.S. Fischer, Phys. Rev. **B19**, 402 (1979). R.A.T. de Lima and C. Tsallis, Phys. Rev. **B27**, 6896 (1983).
[7] - L.N. Bulaevskii, A.I. Buzdin, and D.I. Khomskii, Solid State Commun. **27**, 5 (1978).
[8] - M. C. Cross, Phys. Rev. **B20**, 4606 (1979).
[9] - H. Bethe, Z. Physik **71**, 205 (1931).
[10] - F.D. Haldane - Phys. Rev. Lett. **50**, 1153 (1983).
[11] -J.C. Bonner and H.W.J. Blöte, Phys. Rev. **B25**, 6959 (1982).
[12] - H. Völlenkle, A. Wittmann and H. Nowotny, Monatsh. Chem. **98**, 1352 (1967).
[13] - M. Braden et al. to appear in Phys. Rev. B (1996).
[14] - J.W. Bray, H.R. Hart, L.V. Interrante, I.S. Jacobs, J.S. Kasper, G.D. Watkins, S.H. Wee and J.C. Bonner, Phys. Rev. Lett. **35**, 744 (1975).
[15] - S. Huizinga, J. Kommandeur, G.A. Savatsky, B.T. Thole, W.J. de Jonge and J. Roos, Phys. Rev. **B19**, 4723 (1979).
[16] - J. Bonner and M.E. Fisher, Phys. Rev. **135**, A640 (1964).
[17] - Q. Liu, S. Ravy, J.P. Pouget, C. Coulon and C. Bourbonnais, Synth. Met. **55-57**, 1840 (1993).
[18] - G. Castilla, S. Chakraverty and V.J. Emery, Phys. Rev. Lett. **75**, 1823 (1995).
[19] - H. van Tol, unpublished.
[20] - W. Palme, G. Ambert, J.P. Boucher, G. Dhalenne and A. Revcolevschi, J. Appl. Phys. **79**, 5384 (1996).
[21] - G. Reményi, S. Sahling, J.C. Lasjaunias, N. Egman, J.P. Brison, A.I. Busdin, G. Dhalenne and A. Revcolevschi, to appear in Phys. Rev. B (1996).
[22] - T.M. Brill, J.P. Boucher, J. Voiron, G. Dhalenne, A. Revcholevschi and J.P. Renard, Phys. Rev. Lett. **73**, 1545 (1994).
[23] - H. Winkelmann, E. Gamper, B. Büchner, M. Braden, A. Revcolevschi, and G. Dhalenne, Phys. Rev. **B51**, 12884 (1995).
[24] - Q.J. Harris, Q. Feng, R.J. Birgeneau, K. Hirota, K. Kakurai, J.E. Lorenzo, G. Shirane, M. Hase, and K. Uchinokura, Phys. Rev. **B50**, 1266 (1994).
[25] - J.E. Lorenzo, K. Hirota, G. Shirane, J.M. Tranquada, M. Hase, K. Uchinokura, H. Kojima, I. Tanaka, and Y. Shibuya, Phys. Rev. **B50**, 1278 (1994).
[26] - K. Hirota, D. E. Cox, J. E. Lorenzo, G. Shirane, J. M. Tranquada, M. Hase, K. Uchinokura, H. Kojima, Y. Shibuya, and I. Tanaka, Phys. Rev. Lett. **73**, 736 (1994).
[27] - J.P. Pouget, L.P. Regnault, M. Aïn, B. Hennion, J.P. Renard, P. Veillet, G. Dhalenne and A. Revcolevschi, Phys. Rev. Lett. **72**, 4037 (1994).
[28] - L.P. Regnault, M. Aïn, B. Hennion, G. Dhalenne, and A. Revcolevschi, Phys. Rev. **B53**, 5579 (1996).

[29] - O. Kamimura, M. Terauchi, M. Tanaka, O. Fujita, and J. Akimitsu, J. Soc. Phys. Jpn. **63**, 2467 (1994).
[30] - K. Hirota, G. Shirane, Q. J. Harris, Q. Feng, R. J. Birgeneau, M. Hase, and K. Uchinokura, Phys. Rev. **B52**, 15412 (1995).
[31] - J.P. Schoeffel, J.P. Pouget, G. Dhalenne and A. Revcolevschi, to appear in Phys. Rev. **B** (1996).
[32] - K. Hirota, R.J. Birgeneau, M. Hase, H. Kojima, J.E. Lorenzo, Y. Shibuya, G. Shirane, I. Tanaka, J.M. Tranquada, and K. Uchinokura, Physica **B213&214**, 284 (1995).
[33] - B. Hennion et al. (unpublished).
[34] - M. Nishi, O. Fujita, and J. Akimitsu Physica **B210**, 149 (1995); Phys. Rev. **B50**, 6508 (1994).
[35] - M. Arai, M. Fujita, K. Ubukata, T. Bokui, K. Tabata, H. Ohta, M. Motokawa, T. Otomo, K. Ohyama, M. Mino, J. Akimitsu, and O. Fujita, J. Phys. Soc. Jpn **63**, 1661 (1994).
[36] - Z.V. Popovic, S. D. Devic, V.N. Popov, G. Dhalenne and A. Revcolevschi, Phys. Rev. **B52**, 4185 (1995).
[37] - M. Hase, I. Terasaki, K. Uchinokura, M. Tokunaga, N. Miura, and H. Obara, Phys. Rev. **B48**, 9616 (1993).
[38] - M. Poirier, M. Castonguay, A. Revcolevschi, and G. Dhalenne, Phys. Rev. **B51**, 6147 (1995).
[39] - M. Saint-Paul, G. Remenyi, N. Hegmann, P. Monceau, G. Dhalenne, and A. Revcolevschi, Phys. Rev. **B52**, 15298 (1995).
[40] - T. Nakano and H. Fukuyama, J. Phys. Soc. Jpn. **49**, 1679 (1980); Phys. Soc. Jpn. **50**, 2489 (1981).
[41] - B. Horowitz, Phys. Rev. Lett. **48**, 742 (1981).
[42] - A.I. Buzdin and S.V. Polonskii, Sov. Phys. JETP **66**, 422 (1987).
[43] - M. Fujita and K. Machida, Phys. Soc. Jpn. **53**, 4395 (1984); Phys. Rev. **B30**, 5284 (1984); J. Phys. C: Solid State Phys. **21**, 5813 (1988).
[44] - V. Kiryukhin and B. Keimer, Phys. Rev. **B52**, R704 (1995).
[45] - V. Kiryukhin, B. Keimer, J. P. Hill, and A. Vigliante, preprint 1996.
[46] - E. Dagotto and T.M. Rice, Science **271**, 618 (1996).
[47] - M. Nishi, O. Fujita, J. Akimitsu, Phys. Rev. **B50**, 1274 (1994).
[48] - D. Grempel et al. (preprint 1996).
[49] - L.P. Regnault, unpublished.
[50] -P.H.M. van Loosdrecht, J.P. Boucher, G. Martinez, G. Dhalenne and A. Revcholevschi, Phys. Rev. Lett. **76**, 311 (1996).
[51] - P.A. Fleury and R. Loudon, Phys. Rev. **166**, 514 (1968).
[52] - U. Fano, Phys. Rev. **124**, 1866 (1961).
[53] - L.C. Brunel, T.M. Brill, I. Zaliznyak, J.P. Boucher and J.P. Renard, Phys. Rev. Lett. **69**, 1699 (1992).
[54] - S. Oseroff, S.W. Cheong, A. Fondado, B. Aktas and Z. Fisk, J. Appl. Phys. **75** 6819 (1994); H. Otha, S. Imagawa, H. Ushiromaya, M. Motokawa, O. Fujita and J. Akimitsu, J. Phys. Soc. Jpn. **63**, 2870 (1994); H. Otha, S. Imagawa, Y. Yamamoto, M. Motokawa, O. Fujita and J. Akimitsu, J. Magn. Mater. **140-144**, 1685 (1995); M. Honda, T. Shibata, K. Kindo, S. Sugai, T. Takeuchi and H. Hori, J. Phys. Soc. Jpn. **65**, 691 (1996); I. Yamada, M. Nishi and J. Akimitsu, preprint (1996); B. Pilawa, preprint (1996).
[55] - O. Fujita, J. Akimitsu, M. Nishi and K. Kakurai, Phys. Rev. Lett. **74**, 1667 (1995).
[56] - Th. Jolicoeur and O. Golinelli, Phys. Rev. **B50**, 9265 (1994).
[57] - J. Sagi and I. Affleck, preprint (1995).

[58] - Y. Fagot-Revurat, M. Horvatic, C. Berthier, J.P. Boucher, P. Segransan, G. Dhalenene and A. Revcolevschi, preprint (1996).
[59] - M. Itoh, S. Hirashima and K. Motoya, Phys. Rev. **B52**, 3410 (1995).
[60] - H.J. Schulz, Phys. Rev. **B34**, 6372 (1986).
[61] - S. Sachdev, Phys. Rev. **B50**, 13006 (1994).
[62] - J.E. Lorenzo et al., preprint (1996).
[63] - H. Benner and J.P. Boucher in *Magnetic Properties of Layered Transition Metal Compounds* edited by L. de Jongh (Kluwer Academic Press, Deventer, 1989)
[64] - H. Tomita and H. Mashimaya, Prog. Theor. Phys. **48**, 1133 (1972).
[65] - Y. Fagot-Revurat, M. Horvatic, C. Berthier, P. Segransan, G. Dhalenene and A. Revcolevschi, preprint (1996).
[66] - P.H.M. van Loosdrecht, J.P. Boucher, G. Martinez, G. Dhalenne and A. Revcolevschi, J. Appl. Phys.**79**, 5395 (1996).
[67] - W. Palme, G. Ambert, J.P. Boucher, G. Dhalenne and A. Revcolevschi, to appear in Phys. Rev. Lett. (1996).
[68] - H.J. Schulz, in *Low-Dimensional Conductors and Superconductors*, edited by D. Jerome and L.C. Caron (Plenum Publishing Corporation, 1987), page 95.
[69] - J.P. Renard, K. Le Dang, P. Veillet, G. Dhalenne, A. Revcolevschi and L.P. Regnault, Europhys. Lett. **30**, 475 (1995).
[70] - S.B. Oseroff, S.W. Cheong, B. Aktas, M.F. Hundley, Z. Fisk and L.W. Rupp, Jr, Phys. Rev. Lett. **74**, 1450 (1995).

Figure captions:

Fig.1 - (H,T) phase diagram of the spin-Peierls compound $CuGeO_3$ [19, 20] showing the three different phases: uniform (U), dimerised (D) and incommensurate (I). The solid and dashed lines represent second and first order transitions respectively, and (L) the Lifschift point.

Fig.2 - Representation of the crystallographic structure for $CuGeO_3$.

Fig.3 - Magnetic susceptibility of CuGeO3, from [1]. In a) the solid line corresponds to the prediction for Heisenberg AF quantum spin chains [16] with $J_c = 88$ K.

Fig.4 - Magnetization as a function of temperature M(T) for different fields (H//**a**) [19].

Fig.5 - Specific heat as a function of temperature for different fields (H//**c**) [21].

Fig.6 - Hysteresis on magnetization M(H) at the D-U transition (H//**a**) [22].

Fig.7 - Coefficients of the linear thermal expansion along **a**, **b**, **c**, and of the volume as a function of temperature [23].

Fig.8 - Temperature dependence of the lattice constants along **a** [24], and **c** and **b** [26].

Fig.9 - a) Representation of the 3D reciprocal space for $CuGeO_3$; b) Dispersions of the elementary excitations in the D phase, for the two reciprocal directions **b*** and **c*** (see text). The solid curves represent the dispersions observed experimentally.

Fig.10 - Neutron scattering [28]: a) Longitudinal scan through the super-lattice peak [1/2,3,1/2]; b) Temperature dependence of the maximum intensity of this peak, for H = 0 and H = 9.85 T; c) Field dependence of T_{sp} determined from such measurements.

Fig.11 - Thermal dependence of ξ^{-1} along **a***, **b*** and **c***. T_{co} is the temperature at which $\xi_a^{-1} = 1/a$. ξ_b^{-1} and ξ_c^{-1} close to T_{sp} are shown in the inset [31].

Fig.12 - Schematic representation of the low-temperature structure of $CuGeO_3$. Arrows and signs indicate the directions of atomic displacements [26, 13].

Fig.13 - Dispersion relations of phonons in the directions [0 0 1] and [1 0 1] at room temperature [33].

Fig.14 - a) Scans through the [5/2,1,5/2] satellite in the [1 0 1] direction, at 5 K, showing the occurrence of an incommensurate phase above $H_c \sim 11.6$ T [44]; b) Field dependence of the commensurate (closed symbols) and incommensurate (open symbols) showing the step-like behavior at H_c [44].

Fig.15 - Dispersion relations of the elementary excitations in the D phase: along the 3 directions **a***, **b*** and **c***, from [34], and along **c*** and **b***, from [28].

Fig.16 - Raman scattering intensity [50, 66]: a) In the D phase (peaks 1 and 3 correspond to the gap E_{G1} and the maximum E_M of the magnetic dispersion curves); b) In the SRO regime of the U phase (the arrow shows the peak associated with the maximum E'_M of the magnetic spin wave continuum); c) In the HT regime of the U phase showing the development of low-energy fluctuations as T increases; d) At T = 4.2 K for H = 1 and 20 T, i.e., in the D and I phases respectively (as discussed in the text, the peaks shown by the arrow are the signature of (quasi) propagative elementary excitations). In all these figures, the other peaks are associated with phonons [50].

Fig.17 - Effect of a magnetic field on the elementary excitations in the D phase: a) Integrated intensity of the "standard" ESR line (see text) [20]; b) Zeeman splitting of the uniform mode at the Brillouin zone center: $\mathbf{k_0}$ = [0,0,0] [22]; c) Zeeman splitting of the AF mode at $\mathbf{k_{AF}}$ = [0,1,1/2] [28].

Fig.18 - $1/T_1$ data obtained from Cu NQR [59] and NMR [58] data compared with the exp(-Δ/T) contribution (solid line) expected from the low-energy fluctuations resulting from the S = 1 value associated with the elementary excitations in the D phase [58]. In a field (H = 8.4 T), $1/T_1$, which experimentally increases (while the above contribution is predicted to decrease as shown by the dashed line) is better explained by indirect one-excitation processes [58].

Fig.19 - Neutron inelastic scattering [28]: a) Energy scans for T below (1.8 and 13.5 K) and above (15.5 K) T_{sp}; b) Temperature dependence of the SP gap Δ and of the damping parameter Γ (see text).

Fig.20 - Spin-wave continuum of a quantum 1D Heisenberg hamiltonian at T = 0: a) in zero field, b) and c) for the fluctuations parallel $S_{//}$ and perpendicular $S_{\perp}$ to an applied field H, respectively [3] (on the energy axis $H = g\mu_B H/2J_c$).

Fig.21 - Neutron inelastic scattering: Energy scan at T = 15.05 K, i.e., in the U phase, showing the presence of an overdamped continuum at $\mathbf{q_A}$ = 1/2 (the small energy shift is explained by the fact that the measurements have been performed very near T_{sp} and at $\mathbf{q}$ = [0,1.025,1/2], when dispersion in the $\mathbf{b^*}$ direction starts to manifest) [49]. The double-headed arrow evaluates the expected thermal T damping [60].

Fig.22 - ^{63}Cu NMR lineshape (the "echo" intensity) taken at 1.4 K and 169.5 MHz (lower part) and the corresponding local susceptibility distribution $\chi(r)$ (upper part and solid line)- see text and [65].

Fig. 23 - Derivatives of ESR lines taken at the the fixed frequency of 525 Ghz, i.e., in high field. T = 16 K corresponds to the U phase, T = 10 K to T ~ Tsp, T = 8 and 4.2 K to the I phase [67]. At 4.2 K, the hysteresis effect is clearly observed: the solid and broken lines are recorded for increasing and decreasing fields, respectively

Fig. 24 - (x-T) phase diagram of $CuGe_{1-x}Si_xO_3$ obtained from susceptibility measurements on single crystals [69]. SP and Para correspond to the usual D and U phases, while AF is a new ordered AF phase.

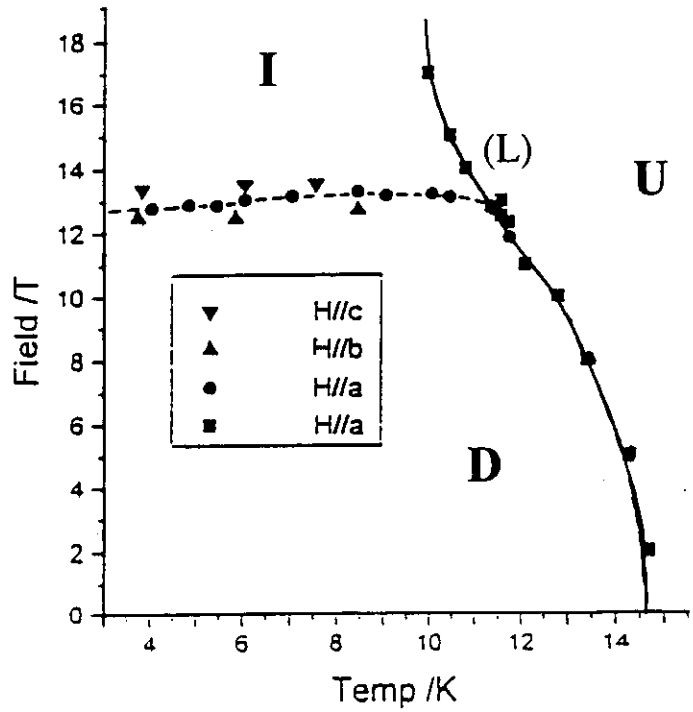

fig 1

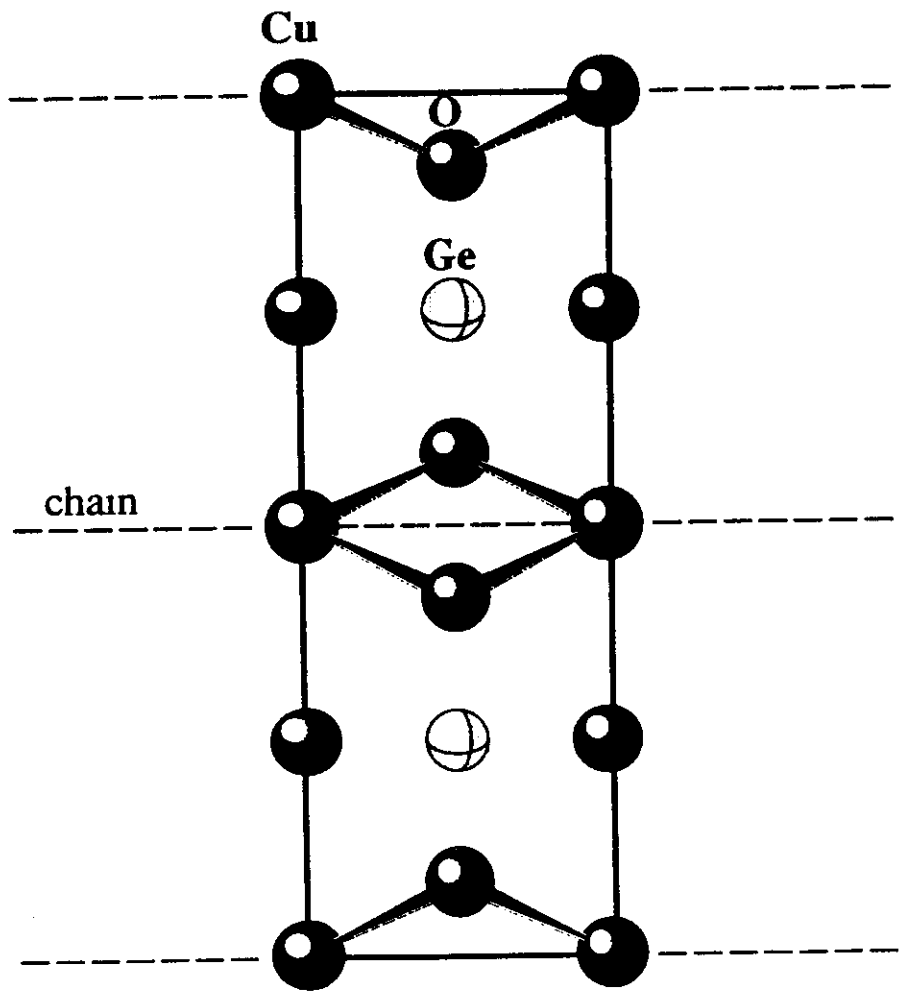

fig. 2

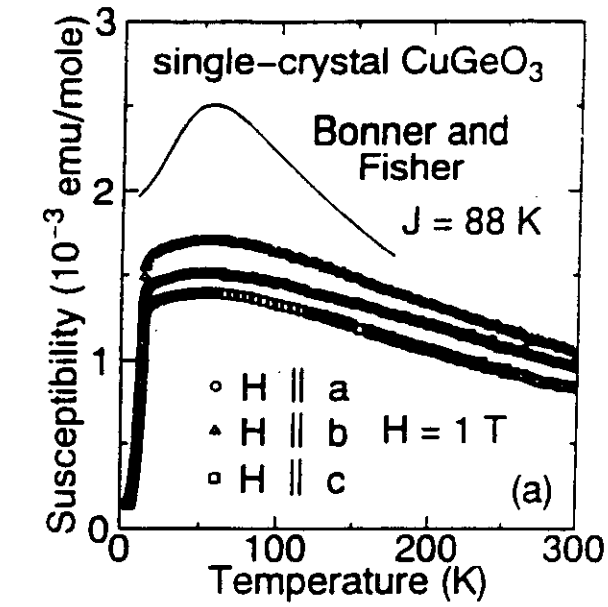
single-crystal $CuGeO_3$
Bonner and Fisher
J = 88 K
H ∥ a
H ∥ b
H ∥ c
H = 1 T
(a)
Susceptibility (10^{-3} emu/mole)
Temperature (K)
0
1
2
3
0
100
200
300

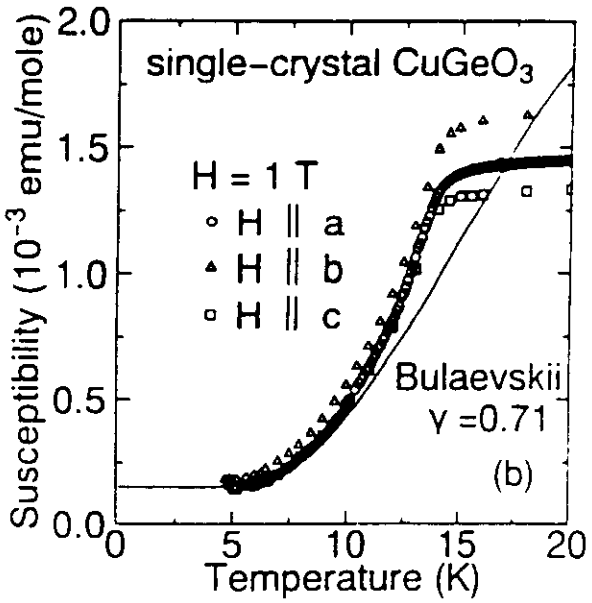
single-crystal $CuGeO_3$
H = 1 T
H ∥ a
H ∥ b
H ∥ c
Bulaevskii
γ =0.71
(b)
Susceptibility (10^{-3} emu/mole)
Temperature (K)
0.0
0.5
1.0
1.5
2.0
0
5
10
15
20

Fig. 3

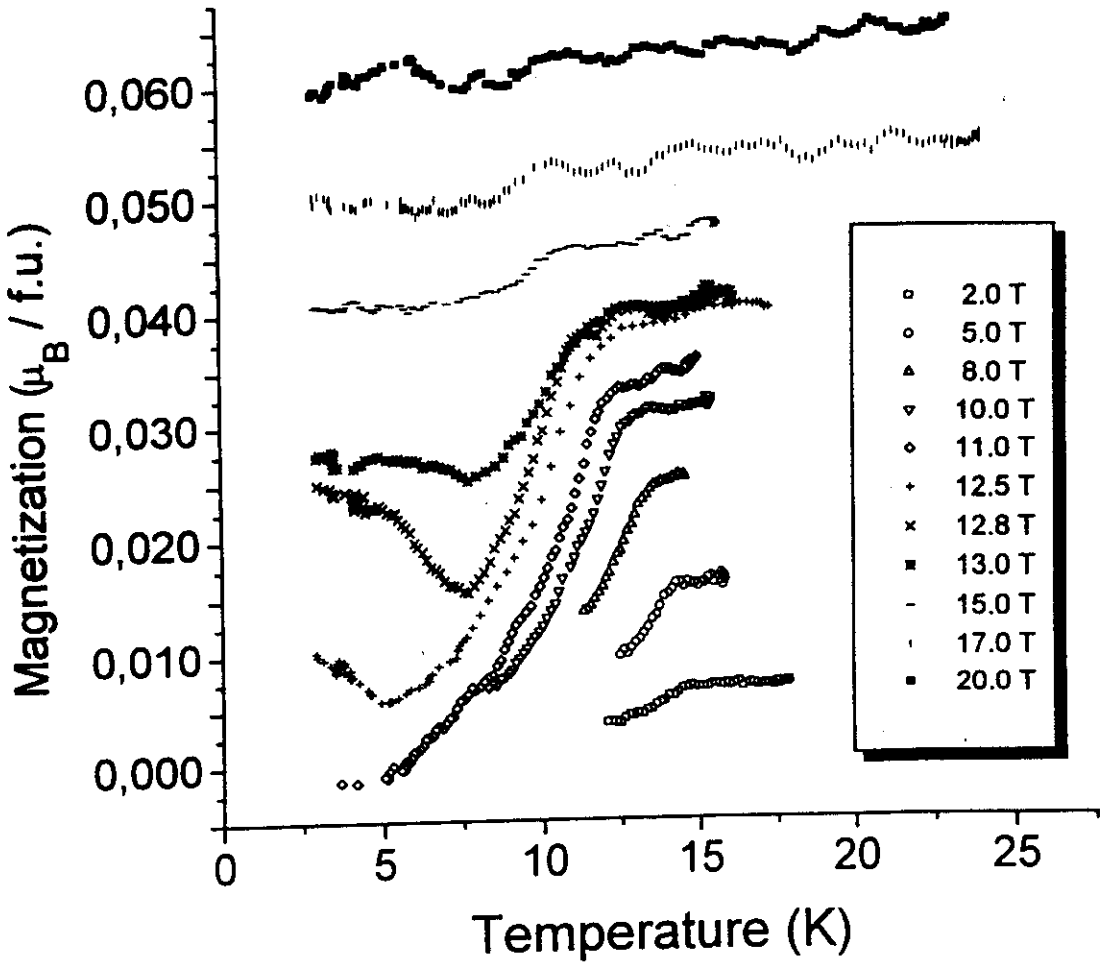
Magnetization (μ_B / f.u.)
0,060
0,050
0,040
0,030
0,020
0,010
0,000
0
5
10
15
20
25
Temperature (K)
2.0 T
5.0 T
8.0 T
10.0 T
11.0 T
12.5 T
12.8 T
13.0 T
15.0 T
17.0 T
20.0 T

fig. 4

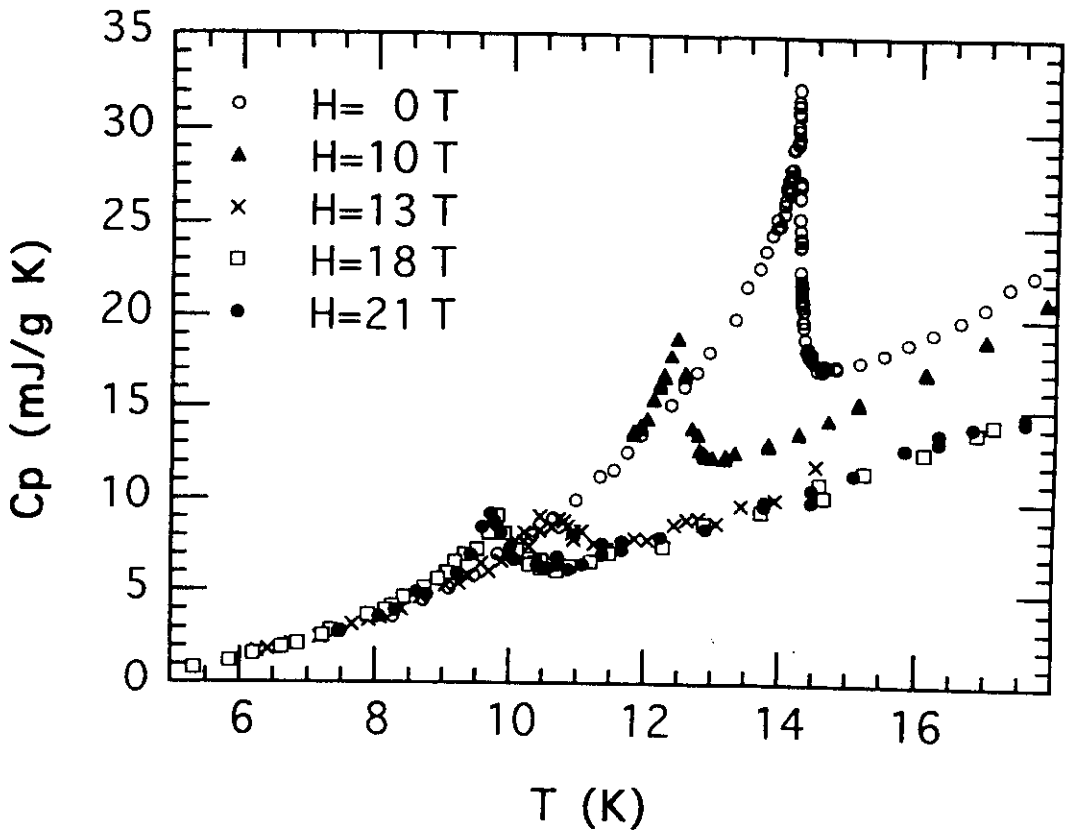
H= 0 T
H=10 T
H=13 T
H=18 T
H=21 T
Cp (mJ/g K)
T (K)
0
5
10
15
20
25
30
35
6
8
10
12
14
16

fig 5

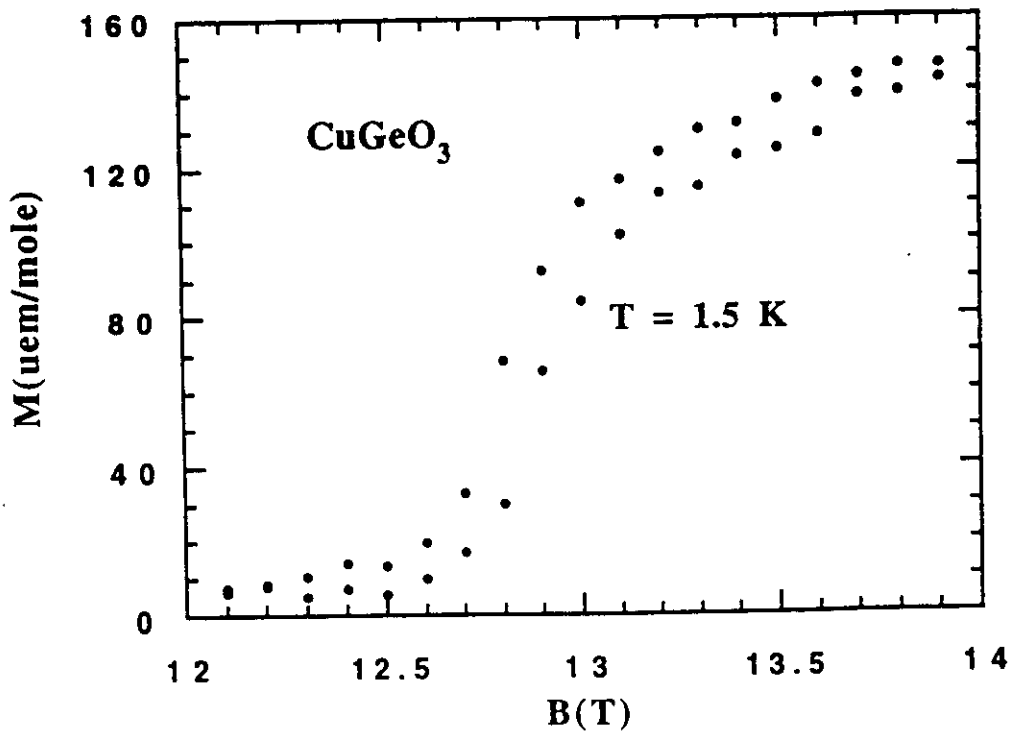

Fig. 6

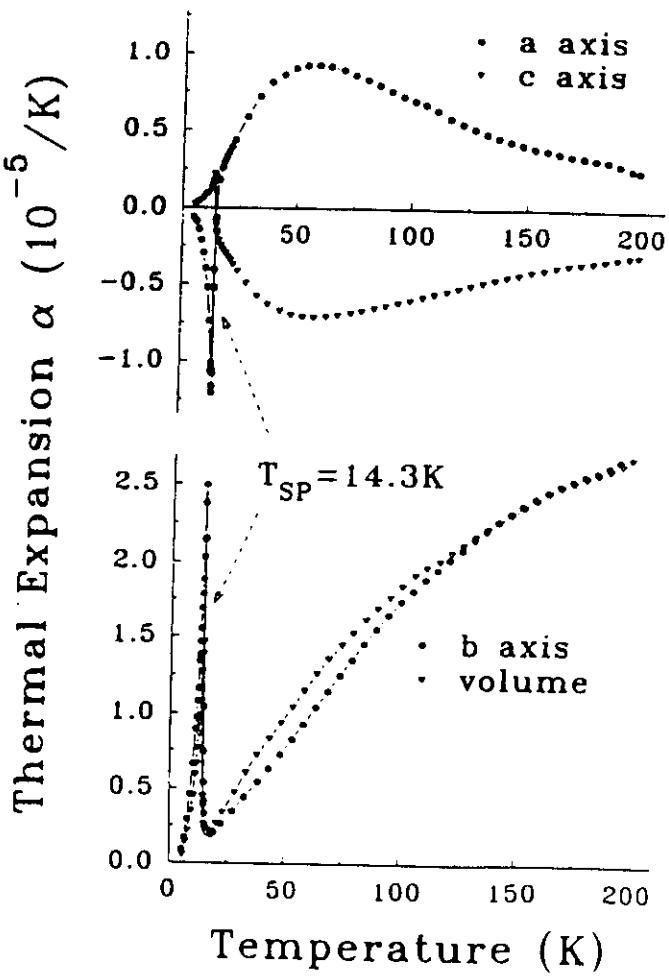
Thermal Expansion α (10⁻⁵/K)
1.0
0.5
0.0
−0.5
−1.0
50
100
150
200
a axis
c axis
T_SP=14.3K
2.5
2.0
1.5
1.0
0.5
0.0
0
50
100
150
200
b axis
volume
Temperature (K)

Fig 7

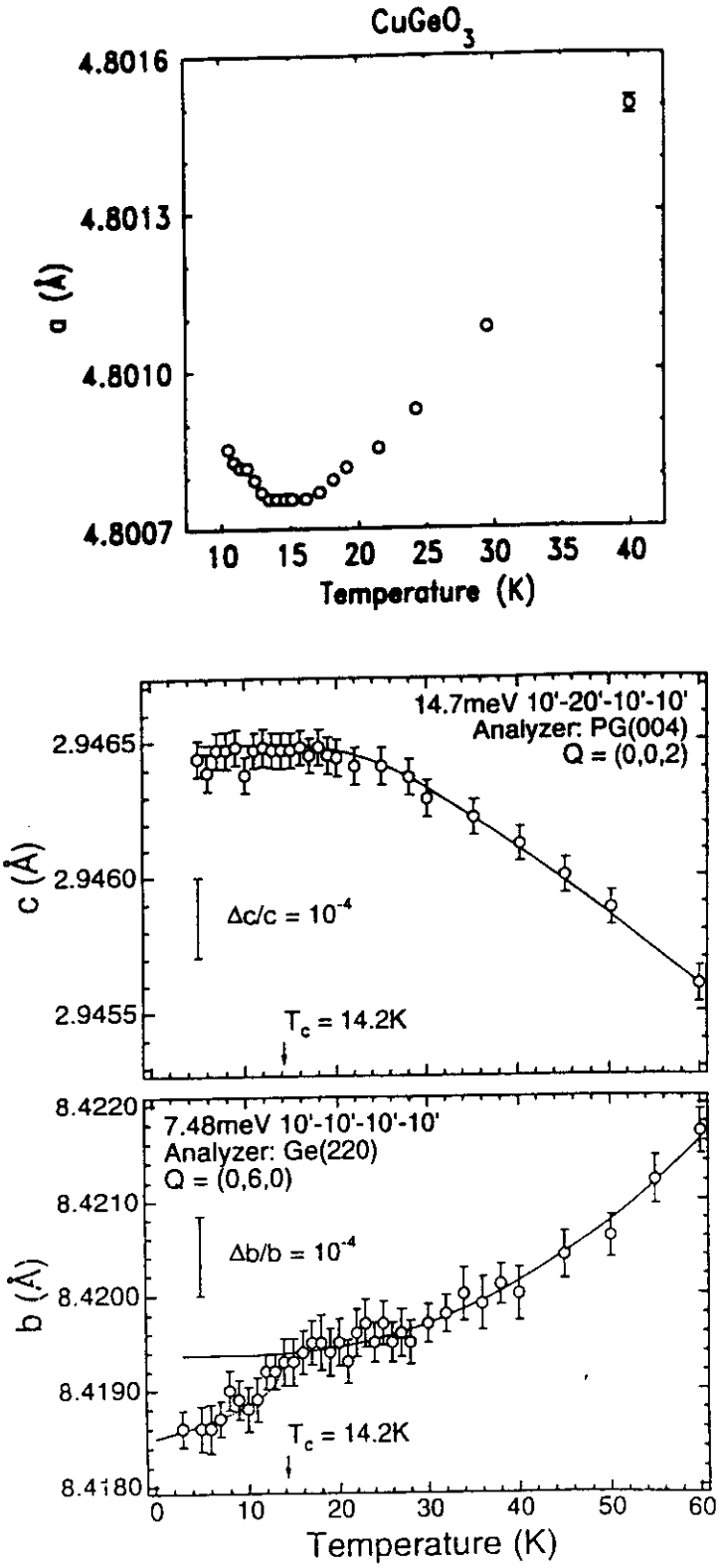
CuGeO3
4.8016
4.8013
4.8010
4.8007
a (Å)
10 15 20 25 30 35 40
Temperature (K)
14.7meV 10'-20'-10'-10'
Analyzer: PG(004)
Q = (0,0,2)
2.9465
2.9460
2.9455
c (Å)
Δc/c = 10-4
Tc = 14.2K
7.48meV 10'-10'-10'-10'
Analyzer: Ge(220)
Q = (0,6,0)
8.4220
8.4210
8.4200
8.4190
8.4180
b (Å)
Δb/b = 10-4
Tc = 14.2K
0 10 20 30 40 50 60
Temperature (K)

Fig. 7

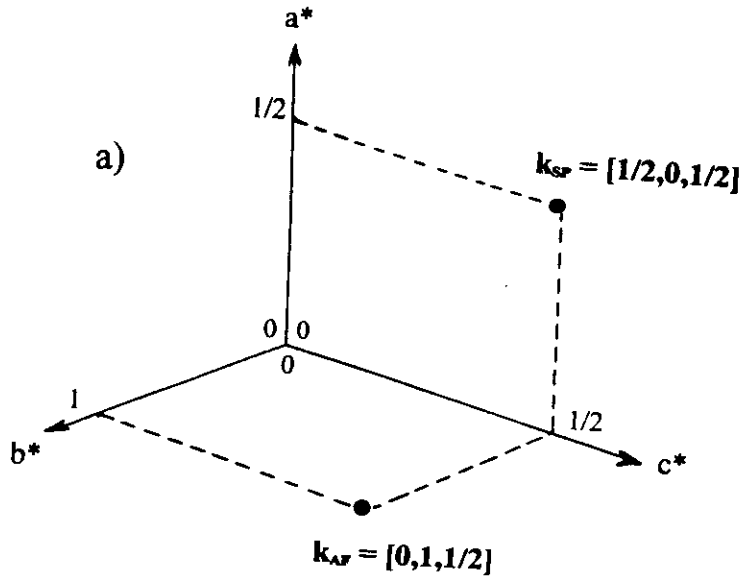
a)
a*
1/2
k_{SF} = [1/2,0,1/2]
0 0
0
1
b*
1/2
c*
k_{AF} = [0,1,1/2]

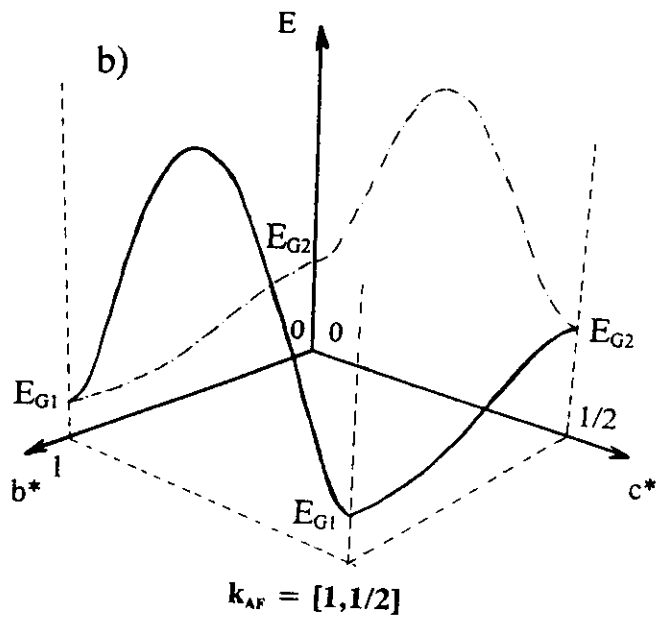
b)
E
E_{G2}
0 0
E_{G2}
E_{G1}
1/2
b*
1
c*
E_{G1}
k_{AF} = [1,1/2]

Fig. 9

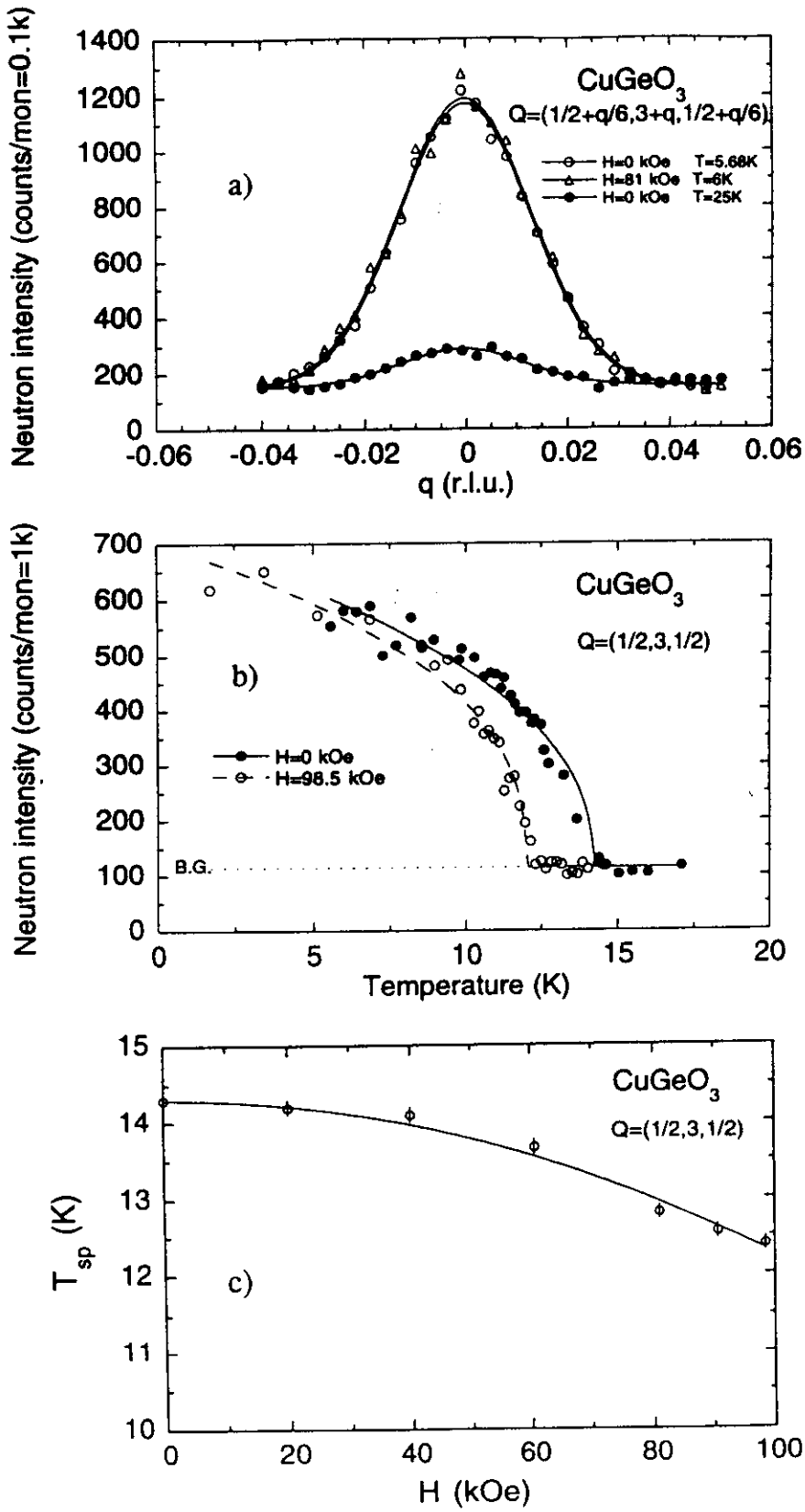
Neutron intensity (counts/mon=0.1k)
1400
1200
1000
800
600
400
200
0
-0.06
-0.04
-0.02
0
0.02
0.04
0.06
q (r.l.u.)
a)
CuGeO3
Q=(1/2+q/6,3+q,1/2+q/6)
H=0 kOe T=5.68K
H=81 kOe T=6K
H=0 kOe T=25K
Neutron intensity (counts/mon=1k)
700
600
500
400
300
200
100
0
0
5
10
15
20
Temperature (K)
b)
CuGeO3
Q=(1/2,3,1/2)
H=0 kOe
H=98.5 kOe
B.G.
T_sp (K)
15
14
13
12
11
10
0
20
40
60
80
100
H (kOe)
c)
CuGeO3
Q=(1/2,3,1/2)

Fig. 10

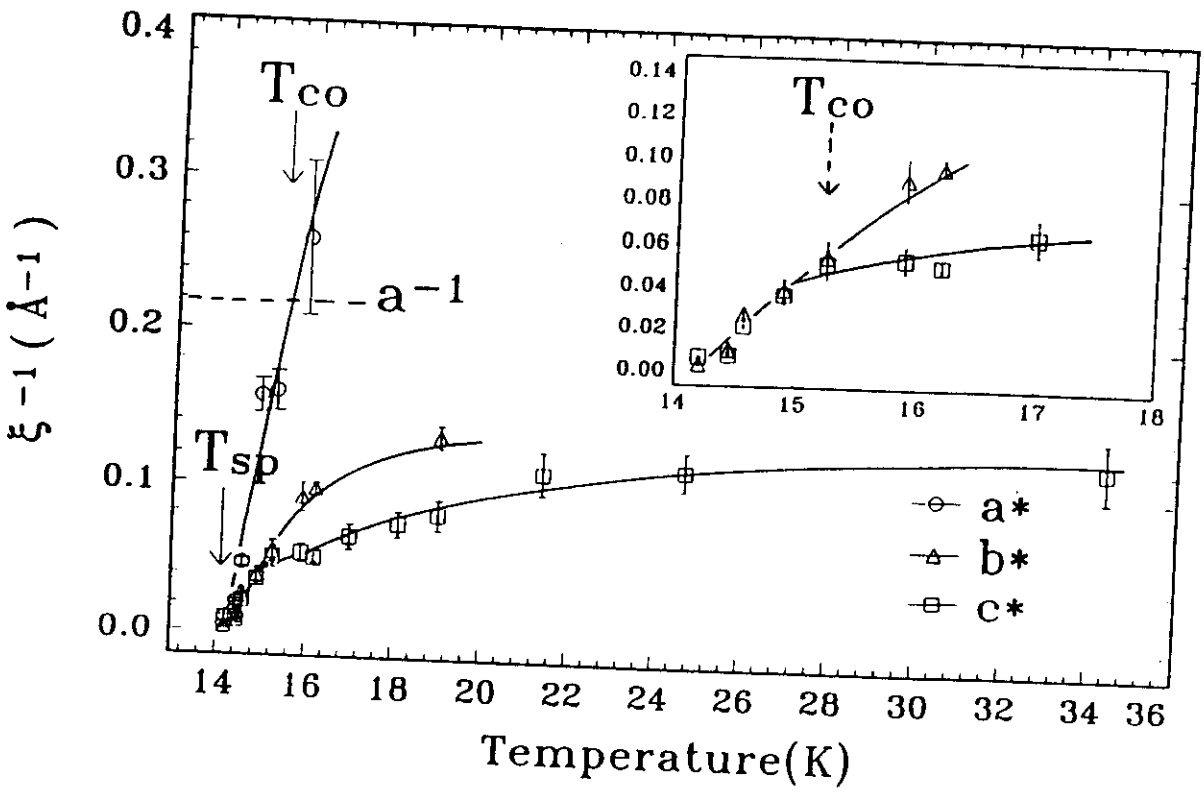
0.4
0.3
0.2
0.1
0.0
ξ^{-1} (Å^{-1})
T_{co}
a^{-1}
T_{sp}
a*
b*
c*
14 16 18 20 22 24 26 28 30 32 34 36
Temperature(K)
0.14
0.12
0.10
0.08
0.06
0.04
0.02
0.00
T_{co}
14 15 16 17 18

Fig. 11

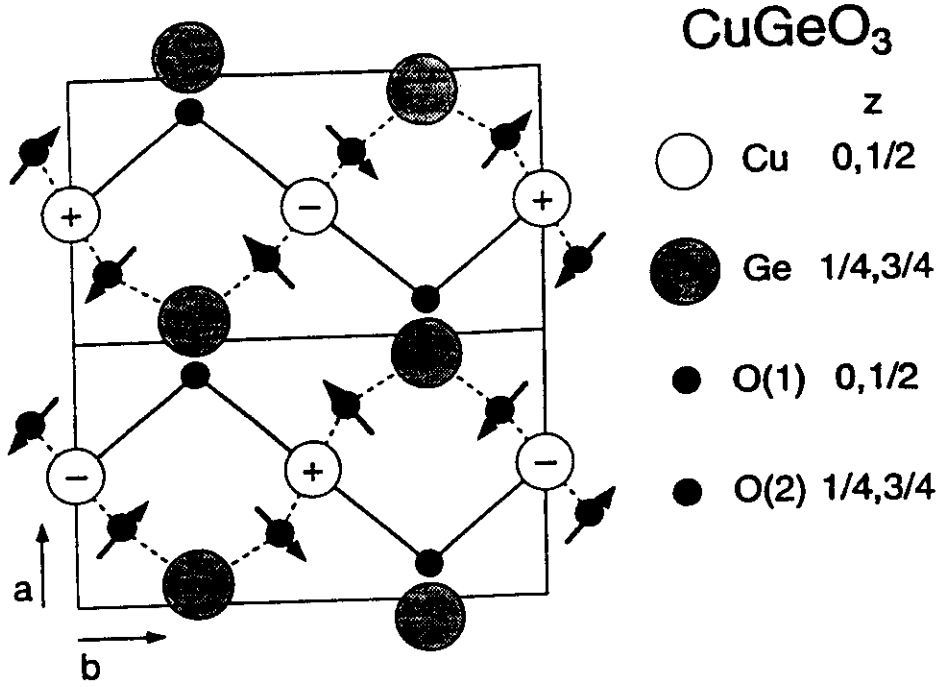

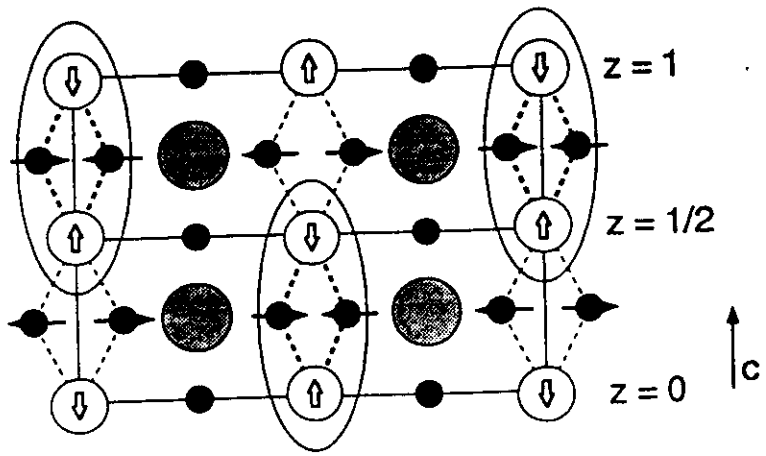

fig. 12

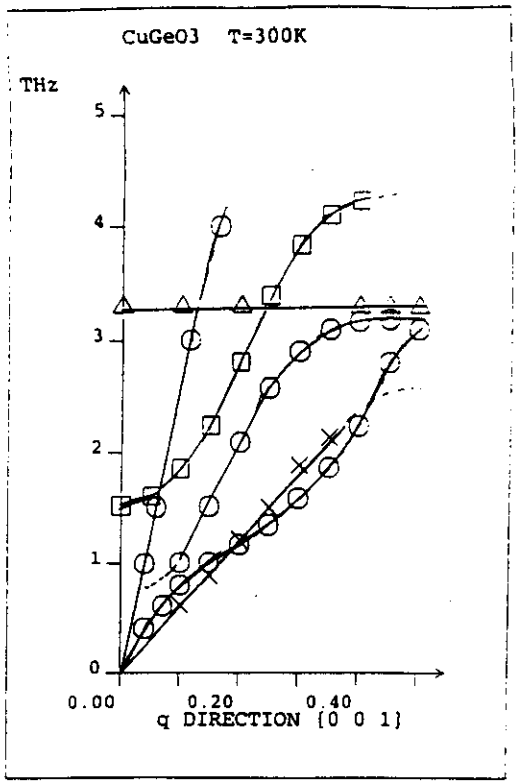
CuGeO3 T=300K
THz
5
4
3
2
1
0
0.00
0.20
0.40
q DIRECTION [0 0 1]

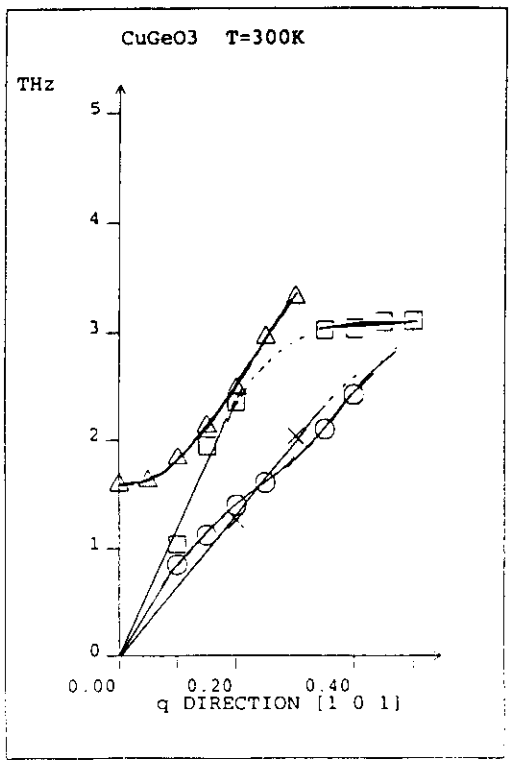
CuGeO3 T=300K
THz
5
4
3
2
1
0
0.00
0.20
0.40
q DIRECTION [1 0 1]

Fig. 13

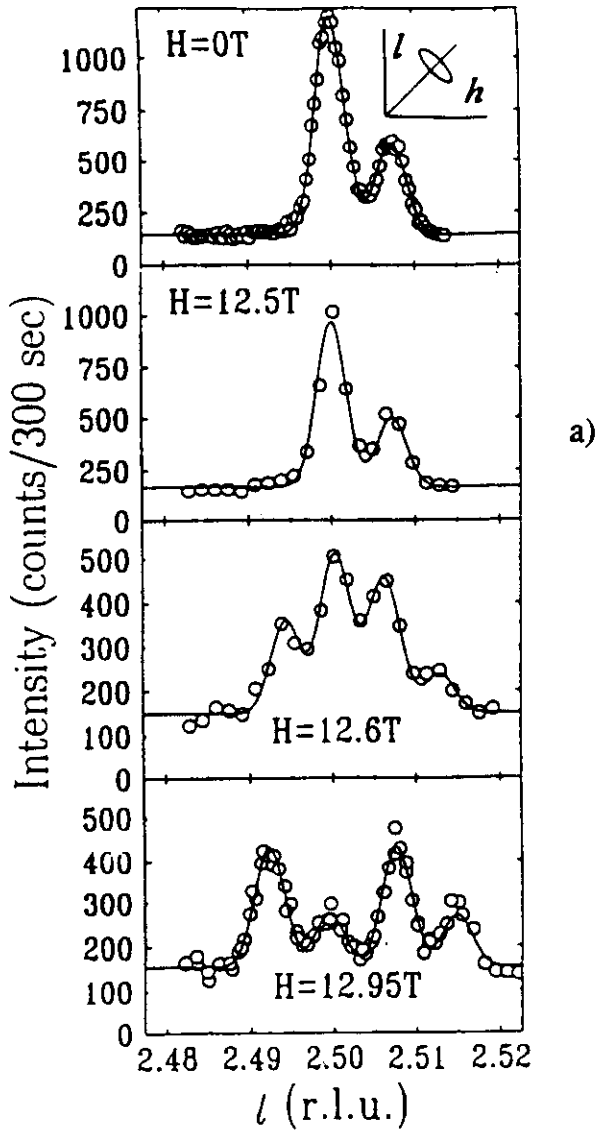
H=0T
H=12.5T
H=12.6T
H=12.95T
Intensity (counts/300 sec)
l (r.l.u.)
a)

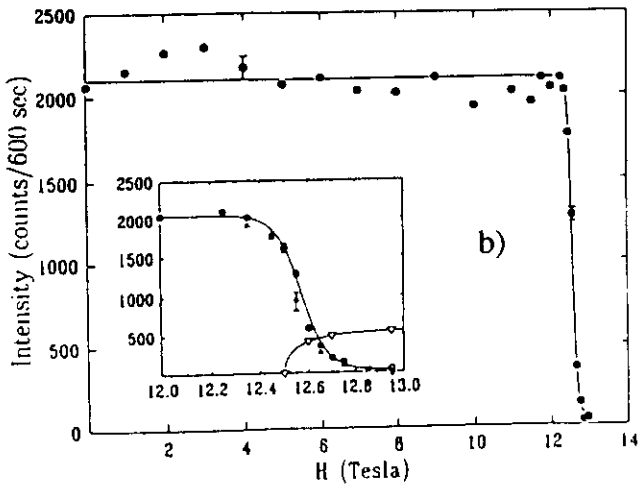
Intensity (counts/600 sec)
H (Tesla)
b)

Fig. 14

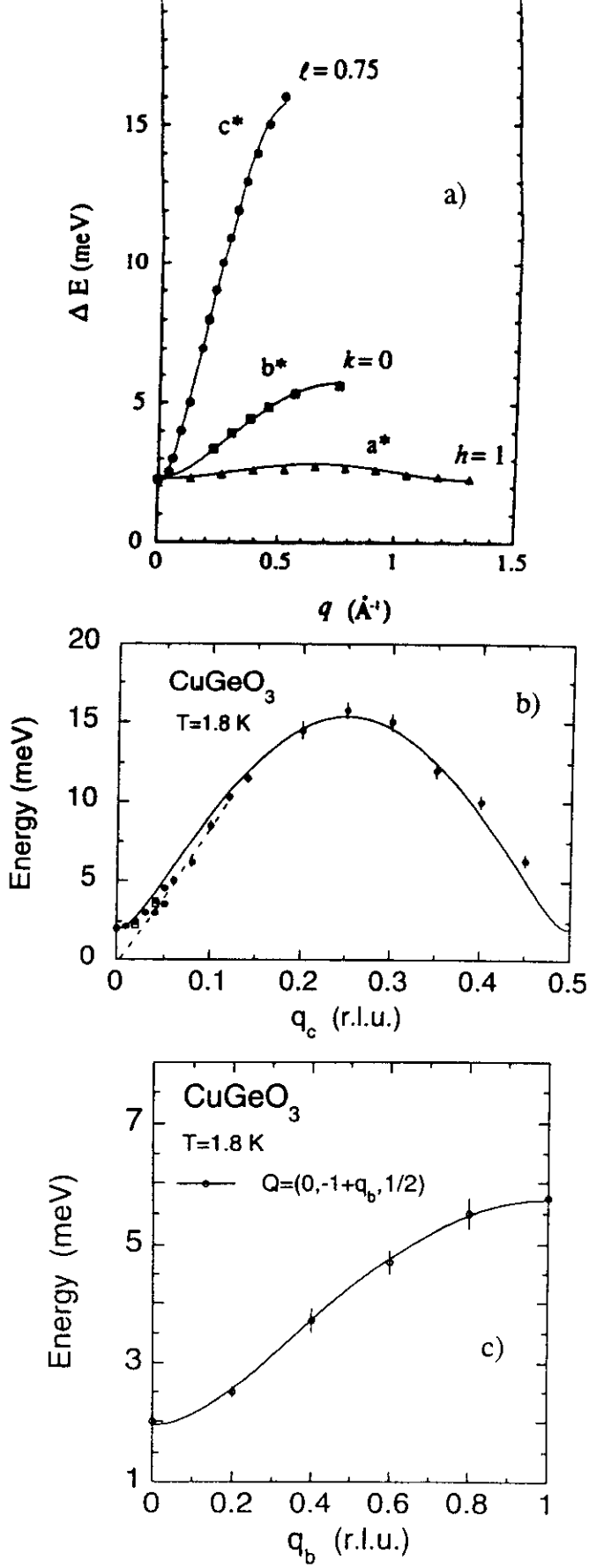
ℓ = 0.75
c*
a)
ΔE (meV)
b*
k = 0
a*
h = 1
q (Å⁻¹)
CuGeO3
T=1.8 K
b)
Energy (meV)
qc (r.l.u.)
CuGeO3
T=1.8 K
Q=(0,-1+qb,1/2)
c)
Energy (meV)
qb (r.l.u.)

Fig. 15

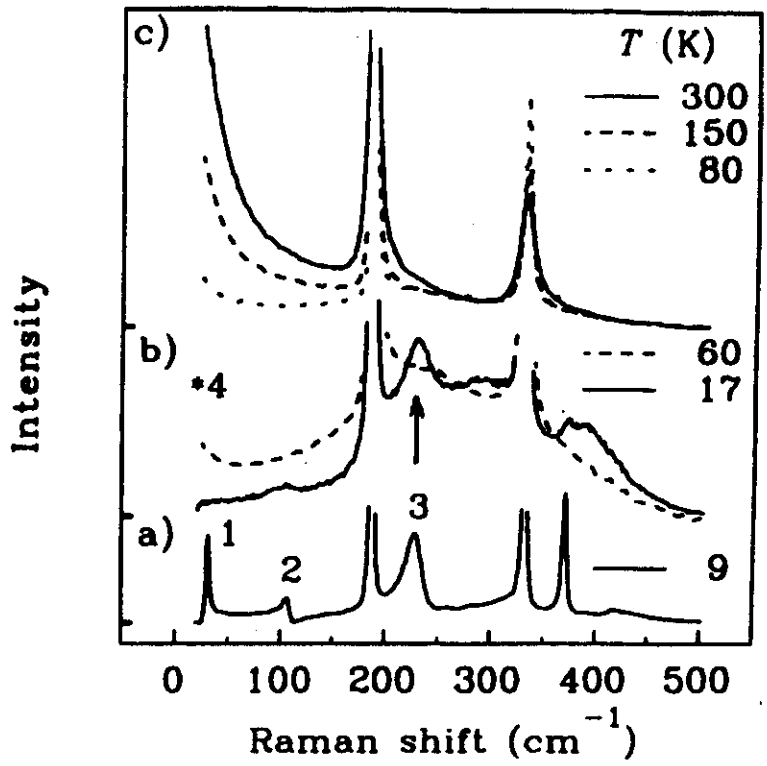
c)
T (K)
300
150
80
b)
*4
60
17
a)
1
2
3
9
Intensity
0
100
200
300
400
500
Raman shift (cm^{-1})

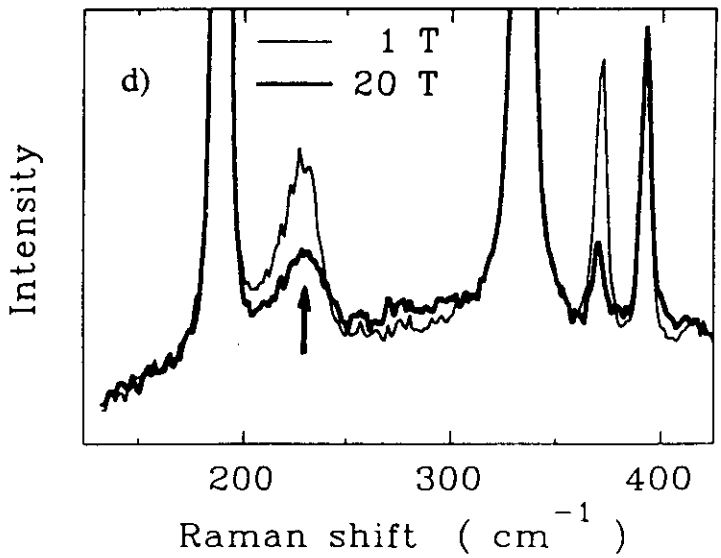
d)
1 T
20 T
Intensity
200
300
400
Raman shift (cm^{-1})

fig 16

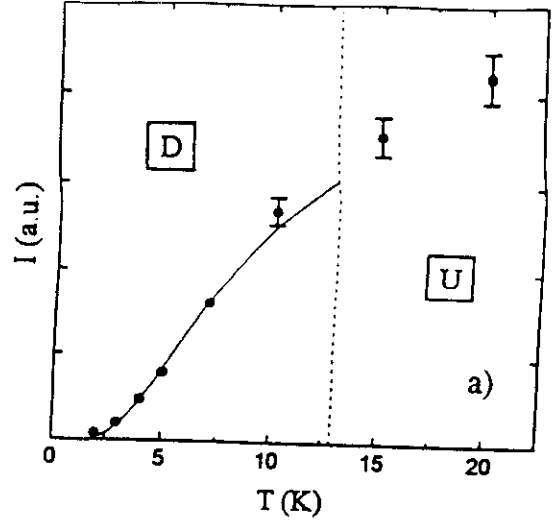
D
U
a)
I (a.u.)
T (K)
0
5
10
15
20

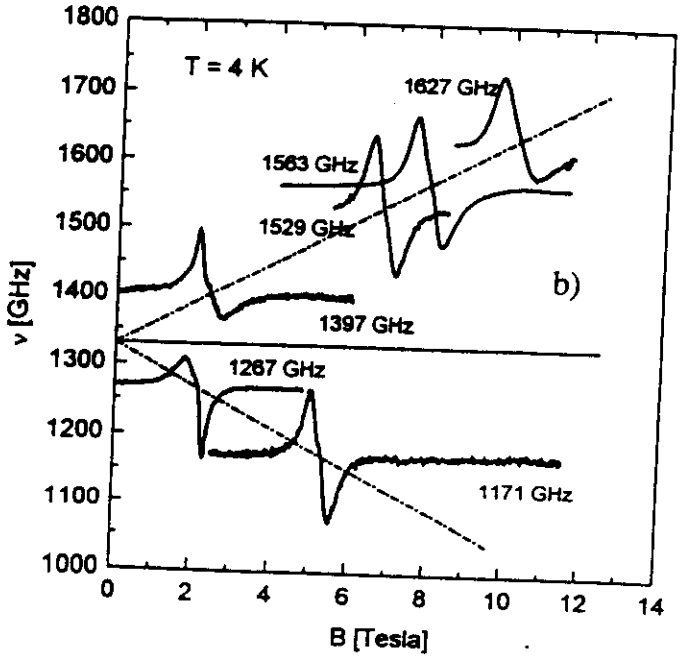
T = 4 K
1627 GHz
1563 GHz
1529 GHz
1397 GHz
1267 GHz
1171 GHz
b)
ν [GHz]
B [Tesla]
1800
1700
1600
1500
1400
1300
1200
1100
1000
0
2
4
6
8
10
12
14

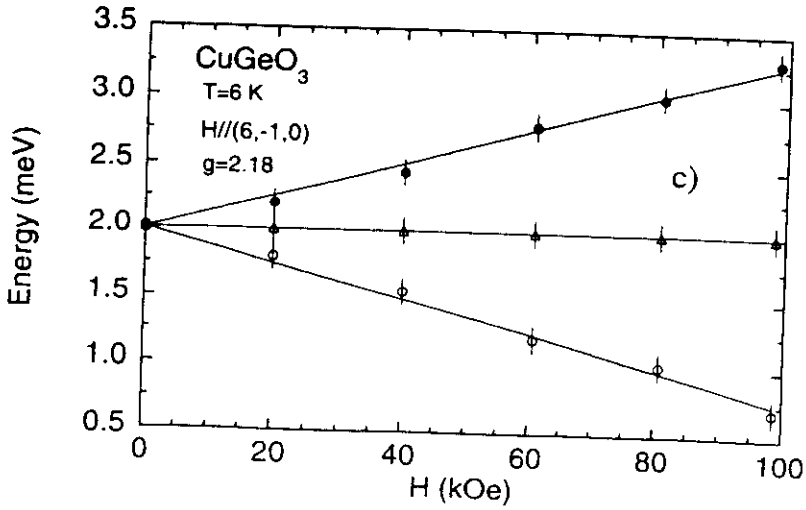
CuGeO3
T=6 K
H//(6,-1,0)
g=2.18
c)
Energy (meV)
H (kOe)
3.5
3.0
2.5
2.0
1.5
1.0
0.5
0
20
40
60
80
100

Fig. 17

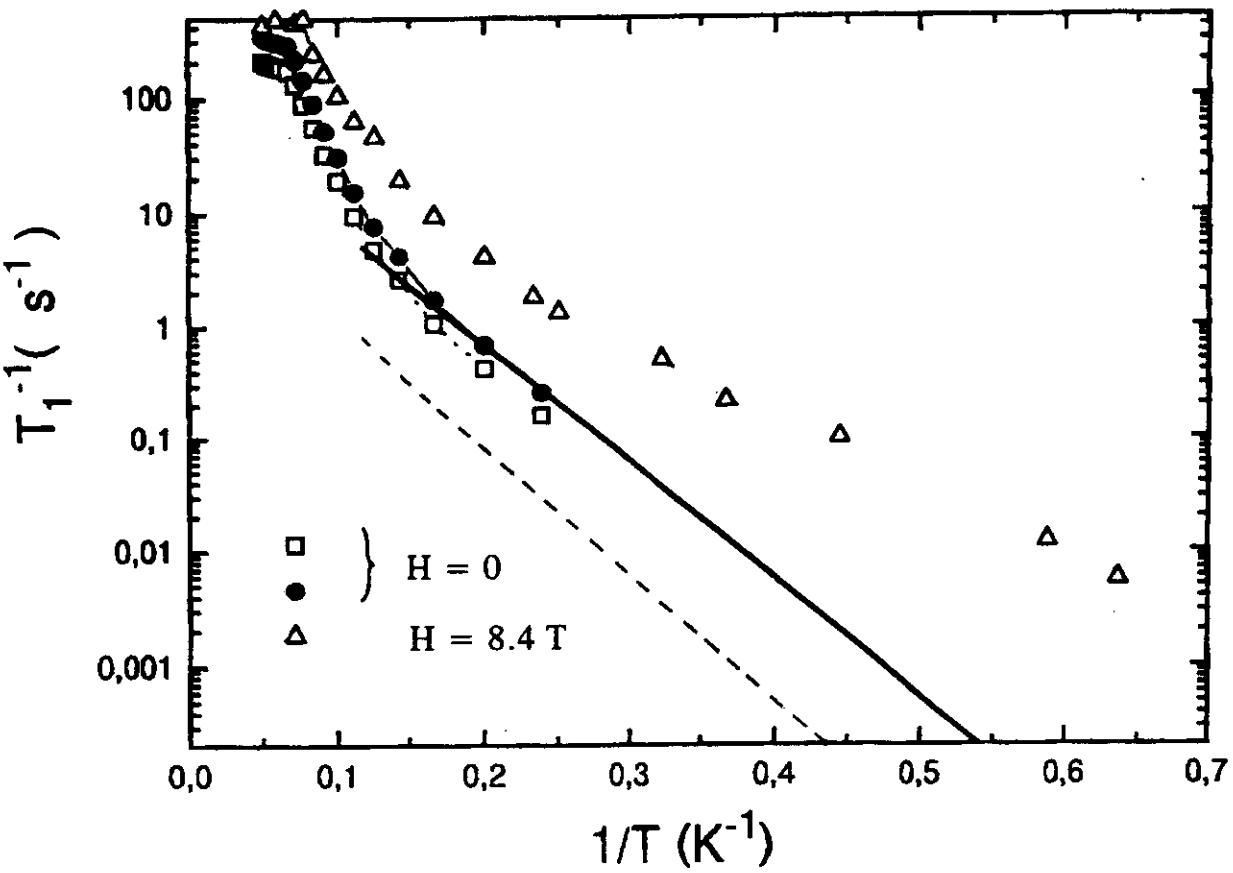

Fig. 18

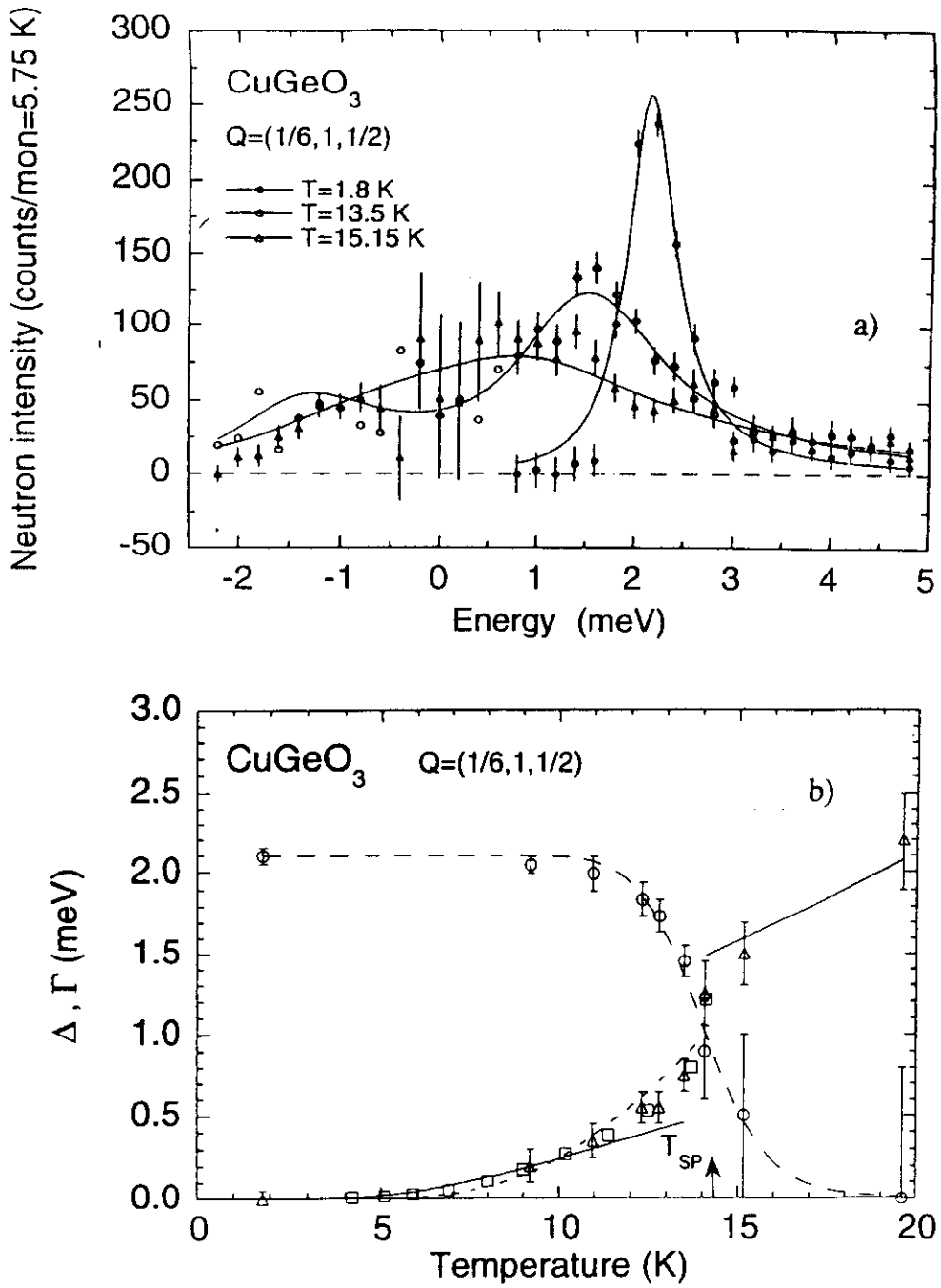
Neutron intensity (counts/mon=5.75 K)
CuGeO3
Q=(1/6,1,1/2)
T=1.8 K
T=13.5 K
T=15.15 K
a)
Energy (meV)
CuGeO3 Q=(1/6,1,1/2)
b)
Δ, Γ (meV)
T_SP
Temperature (K)

Fig. 19

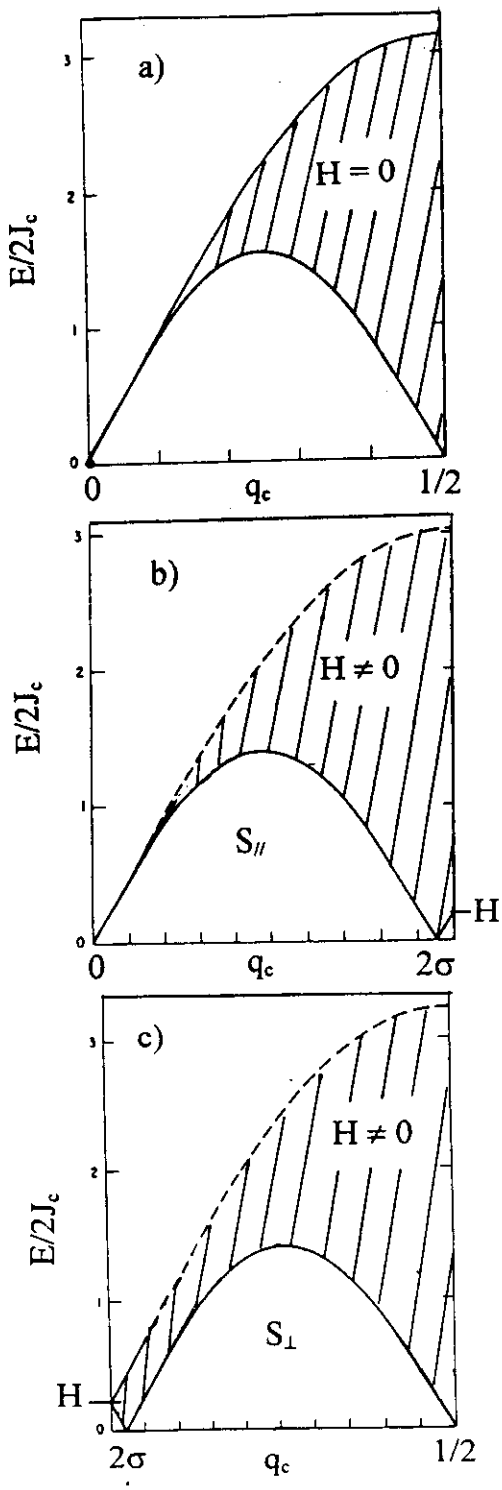

fig. 10

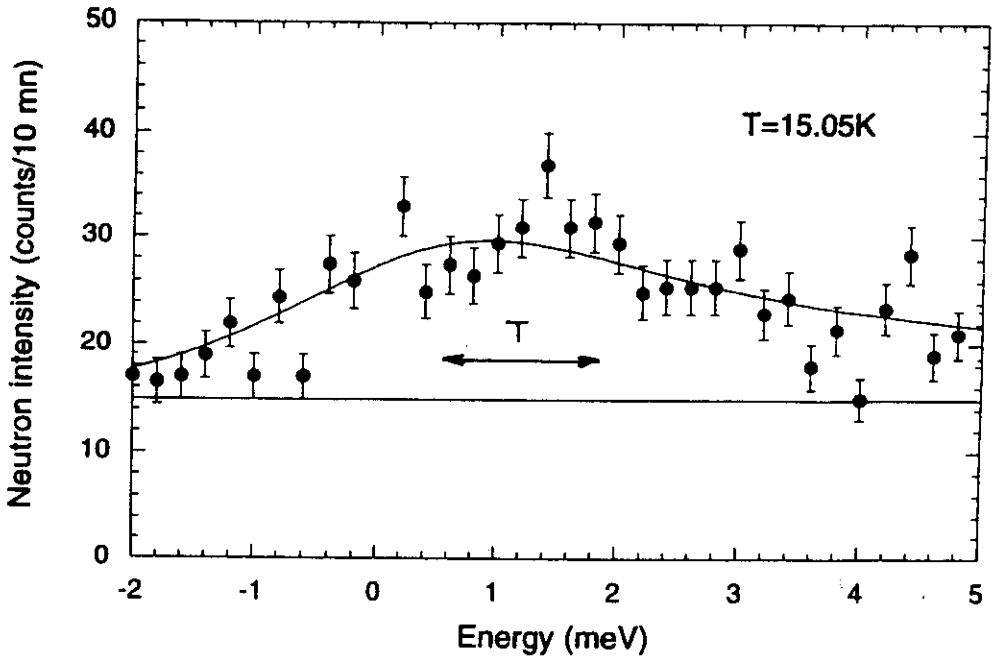
T=15.05K
Neutron intensity (counts/10 mn)
Energy (meV)
50
40
30
20
10
0
-2
-1
0
1
2
3
4
5
T

Fig. 21

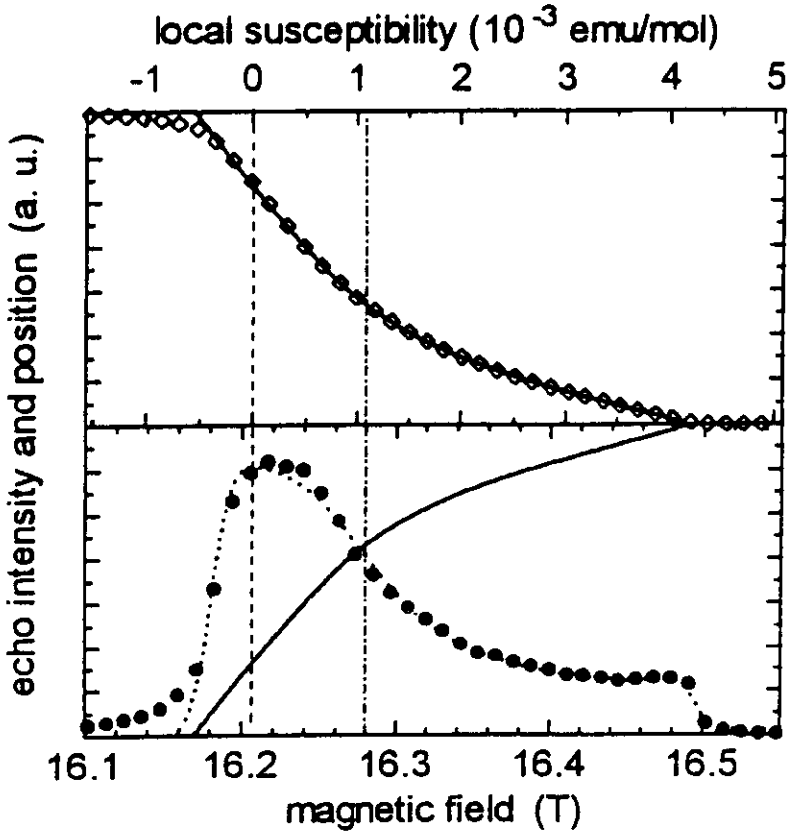
local susceptibility (10^{-3} emu/mol)
-1
0
1
2
3
4
5
echo intensity and position (a. u.)
16.1
16.2
16.3
16.4
16.5
magnetic field (T)

fig 22

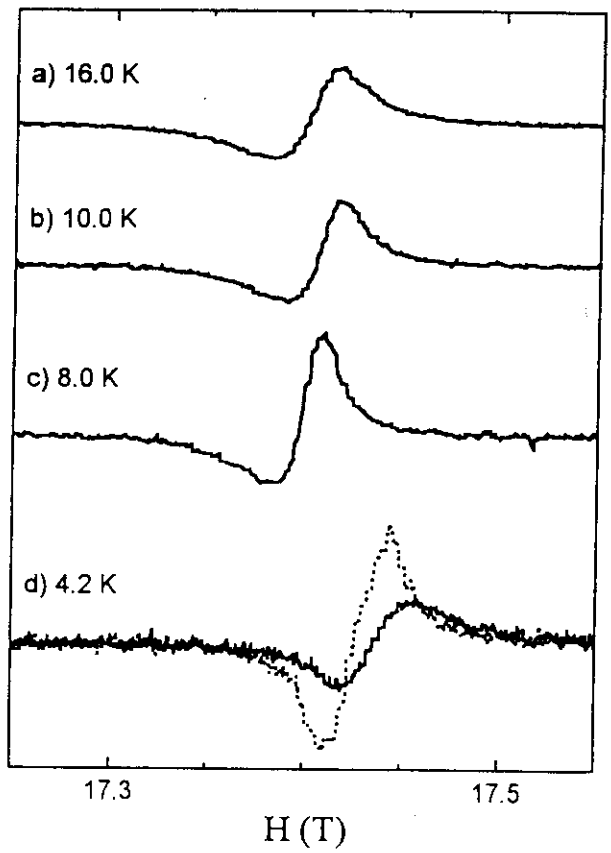

Fig. 23

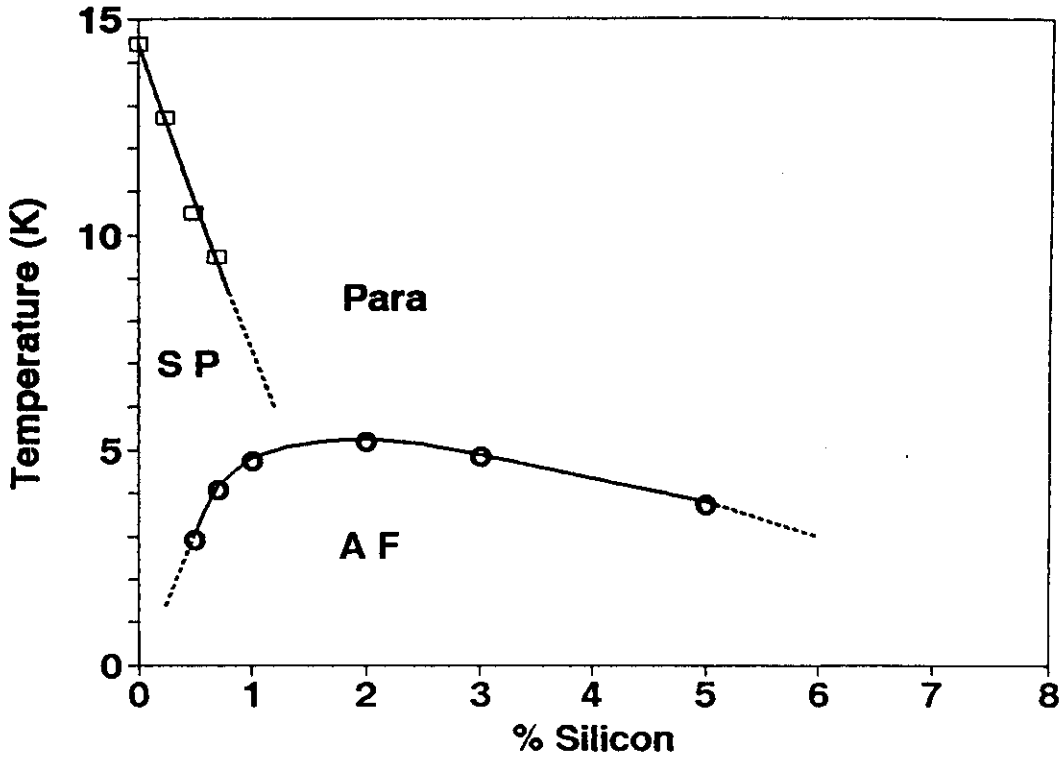

fig. 24